



GISUP 2021, International
The 23th International Symposium of
Geospatial Information Science and Urban Planning



From Nabekanmuri Mountain (Nagasaki Harbor), Nagasaki, Japan

December 18, 2021

Online Web Conference
Bunkyo Campus, Nagasaki University,
1-14 Bunkyo Machi, Nagasaki 852-8521, Japan
Organizing Committee of GISUP2021, International



GISUP 2021, International

The 23th International Symposium of
Geospatial Information Science and Urban Planning

December 18, 2021

Online Web Conference

Bunkyo Campus, Nagasaki University,
1-14 Bunkyo Machi, Nagasaki 852-8521, Japan

Organizing Committee of GISUP2021, International

Published by

GISUP, INTERNATIONAL

1-14 Bunkyo-Machi, Nagasaki City, 852-8521, Japan

GISUP 2021, International

The 23th International Symposium of Geospatial Information Science and Urban Planning

Copyright (c) 2021 by GISUP, INTERNATIONAL

All rights reserved. This book, or parts thereof, may not be reproduced in any form or by any means, electronic or mechanical, including photocopying, recording or any information storage and retrieval system now known or to be invented, without written permission from the Publisher.

ISBN-978-4-9907633-7-4

This collection of papers was produced with the support by JSPS Grant-in-Aid for Scientific Research (C) (No. 20K12322).

Typeset by

Secretariat of Organizing Committee

office@gisup.org <http://gisup.org>

Printed by

GA Creous Co., Ltd.

Kinko's AMU PLAZA Nagasaki Center, Japan

Welcome to GISUP 2021

Welcome to GISUP2021 in Nagasaki, Japan

Dear Colleagues,

We are very glad to host the GISUP2021 conference in Nagasaki. The COVID-19 pandemic has continued for more than a year and a half, and it has been difficult to meet, so this conference will be held on-line. We will prepare a program that will allow colleagues to participate meaningfully. There is a word “如己愛人” in Nagasaki meaning “love your neighbor as yourself”. This word was coined by Dr. Nagai Takashi, who was himself exposed to the atomic bomb detonation but continued to administer treatment to other people. This is an important word now because we are in a time when we need to care for each other by maintaining social distance.



When this pandemic is over, please visit Nagasaki. There are a lot of delicious foods and beautiful scenery. Let's enjoy a meal and converse together.

We are looking forward to meeting you at GISUP2021.

Best regards
General Chair, Prof. Rieko Nakao

A handwritten signature in black ink that reads "Rieko N".

ORGANIZING COMMITTEE

Conference Chair:

Rieko Nakao, Nagasaki University, Japan
(rieiko@nagasaki-u.ac.jp)

Vice Chair (Taiwan): Cheng-di Dong, National Kaohsiung Marine University, TAIWAN
(cddong@webmail.nkmu.edu.tw)

Vice Chair (Korea): Heui-Chae Jin, Baekseok University, Korea
(hcjin@bu.ac.kr)

Vice Chair (Japan): Takahito Ueno, Sojo University, Japan
(ueno@ed.sojo-u.ac.jp)

Vice Chair (China): Mingyi Du, Beijing University of Civil Engineering and Architecture, China
(dumingyi@bucea.edu.cn)

Members:

Jui-Chung Kao, National Kaohsiung University of Science and Technology, Taiwan
(jckao@wnkust.edu.tw)

Hui-Lun Yu, National Kaohsiung University of Science and Technology, Taiwan
(hlyu@nkust.edu.tw)

Xianglei Liu, Beijing University of Civil Engineering and Architecture, China
(liuxianglei@bucea.edu.cn)

He Huang, Beijing University of Civil Engineering and Architecture, China
(huanghe@bucea.edu.cn)

Ming Huang, Beijing University of Civil Engineering and Architecture, China
(huangming@bucea.edu.cn)

Liang Huo, Beijing University of Civil Engineering and Architecture, China
(huoliang@bucea.edu.cn)

Dean Luo, Beijing University of Civil Engineering and Architecture, China
(luodean@bucea.edu.cn)

Changfeng Jing, Beijing University of Civil Engineering and Architecture, China
(jingcf@bucea.edu.cn)

Takeshi Yamaguchi, University of the Ryukyus, Japan
(t-yama@edu.u-ryukyu.ac.jp)

Chang-Hahk Hahm, Inha Technical College, Korea
(chhahm@inhate.ac.kr)

Eung-Nam Kim, Inha Technical College, Korea
(kimen@inhatec.ac.kr)

Won-Dae Kim, Inha Technical College, Korea

(kimwd@inhac.ac.kr)

Dongha Lee, Kangwon National University, Korea

(geodesy@kangwon.ac.kr)

Gyeong-Sik Park, Inha Technical College, Korea

(pks@inhac.ac.kr)

Atsuko Yasutake, Nagasaki University, Japan

(yasutake@nagasaki-u.ac.jp)

Akiko Nitta, Kwassui Woman's University, Japan

(n-akiko@kwassui.ac.jp)

Byungdug Jun, Nagasaki University, Japan

(bdjun@nagasaki-u.ac.jp)

GISUP2021 Detailed Program

The 23th International Symposium of
Geospatial Information Science and Urban Planning
(GISUP2023, International)

December 18, 2021

Online Web Conference
Bunkyo Campus, Nagasaki University,
1-14 Bunkyo Machi, Nagasaki 852-8521, Japan

Organized by Organizing Committee of GISUP2021, International
Sponsored by *Nagasaki University, Japan*

Conference Program Contents

The conference consists of information symposium for Geospatial Information Science and Urban Planning (GISUP2021), for scientific sessions on various GIS and urban planning method and system.

Schedule:

Keynote Lecture (13:00- 16:00) after welcoming address

13:05 - 13:25 Prof. Intae Yang of Korea
13:25 - 13:45 Prof. Changfeng Jing of China
13:45 - 14:05 Prof. Cheng-Di Dong of Taiwan
14:05 - 14:25 Prof. Takakazu Ishimatsu of Japan

Presentation (Students) after 5minutes break (*Poster on Screen)

14:30 - 15:45* Presentation-1 (Korea) Tea Yeon Park (Poster)
14:30 - 14:45 Presentation-2 (Japan) Yuka Kawabata (Oral)
14:45 - 15:00 Presentation-3 (Korea) Lee Jae Cheol (Oral)
15:00 - 15:15 Presentation-4 (Japan) Soichiro Higuchi (Oral)
15:15 - 15:30 Presentation-5 (Japan) Tomohisa Matsuzaki (Oral)
15:30 - 15:45 Presentation-6 (Japan) Yuta Umeda (Oral)

Closing Address:

Catalog

- Welcome to GISUP 2021 II
- Organization Committee III

■■■ Keynote Lecture ■■■

- GIS for the Oceans 2
- Visualizing spatiotemporal patterns of city service demand through a space-time exploratory approach 6
- Green catalysis for the organic contaminated sediment remediation by biochar-based catalysts 7
- Compact emergency call to use EOG signal for patient with serious disabilities 13

■■■ Sessions ■■■

- Modeling and Simulation of Rainfall Effect of Autonomous Driving LiDAR Sensor 20
- The supports for the older people living in the community provided by PHNs and CWSs of Community Comprehensive Support Centers in Kyushu, Japan during the COVID-19 pandemic. 25
- Analysis of Positioning Accuracy of GNSS RTK System according to Positioning Environment 29
- Learning Ability of Peace Education Utilized by VR Materials 33
- Representation of Land Subsidence Analysis Using Interferometric SAR and GIS Technology 43
- Colorization of the Historical Aerial Photography with AI “DeOldify” 51

Keynote Lecture

GIS for the Oceans

By Intae Yang

Hello, everyone who attended the 2021 GISUP is welcome.

Founded in 1999, GISUP held a symposium every February and held its 21st GISUP2019 at Kaohsiung University in Taiwan in February 2019. COVID-19 occurred on January 23, 2020, so we couldn't have a symposium. It is fortunate that we can no longer delay the symposium, so we are holding GISUP 2021 through online meeting.

GISUP implies "UP," which means high places, such as "GIS for Urban Planning" and remote exploration, at the beginning stage. But over the past 20 years, our GISUP has developed in a very diverse and progressive direction.

When I saw the launch of the Mars probe "Persistence", which left Earth on July 30, 2020, I thought a lot about Mars exploration. It was thought that the exploration of physical, chemical and biological information on the surface of the sea and the sea floor, which accounts for three-quarters of the Earth we live in, and that "GIS for Ocean" was our future and a legacy to be passed on to our descendants.

On July 31, 2021, UNESCO registered "Korea's tidal flat" as a natural heritage site.

Upon hearing this news, I was interested in cooperative research in the field of GIS and marine science and looked for whether the tidal flat should be scientifically managed.

Some of the results are listed as follows.

1. How will you find, explore, and analyze information to establish a usage plan?
2. What are the management and preservation methods through research on the resilience of the ocean and coast?
3. It was a study on how to alleviate and respond to disasters.

The environment of the sea is unique.

Satellites and aircraft sensors are effective in viewing. However, they cannot look deeply into the water column where the electromagnetic energy they rely on disappears.

In water, sound waves are transmitted farther and faster through seawater than through electromagnetic energy. Most of what can be recognized in the water column and the sea floor must be helped by sound (acoustic remote sensing).

Sound is essential not only to observe the depth of the ocean floor, but also to detect various characteristics of the ocean floor.

GIS in the sea has been transformed into a function that supports multidimensional visualization, simulation, modeling, and decision-making as well as displaying only data. also

GIS is a powerful and unique technology that is important for us to manage the sea in the most sustainable way.

Example of the role of GIS in the sea.

Exploration

There Is Still Much We Don't Know about the Ocean.

Climbing Mt. Everest: More than 1,500 people

Space travel: More than 300 people.

Moon landing: 12 people

Seabed: Only 5% were surveyed, and only two came down to the seabed and returned to the deepest part of the seabed.

Therefore, scientific research on the ocean should be an international priority.

Autonomous underwater vehicle mission plan using GIS.

US Navy Lab at Stennis Space Center in Mississippi.

- The U.S. Navy Research Institute (NRL) creates custom solutions.

- GIS helps overcome computational complexity and difficult visualization for better decision making.

- NRL can integrate existing software with advanced solutions.

Mission planning for underwater vehicles is a complicated process.

Factors such as seawater, ocean currents, water density, waves, boat traffic, and geopolitical boundaries must be considered to make realistic predictions about the feasibility of the mission.

The Virtual Estuary

New GIS tool for exploration and analysis

By Sandra Fox, St. Johns River Water Management District, and Stephen Bourne, PBS&J

A GIS tool developed by a team of experts is helping scientists more effectively study complex coastal and estuary systems.

Coastal flooding from extreme weather events threatens millions of lives and properties along U.S. coastlines every year. Especially hard hit are areas along the Atlantic Ocean and the Gulf of Mexico where over 60 percent of homes and businesses are within 500 feet of the shoreline. Yet, the ability to explore and study complex coastal environments with accuracy and speed has been limited, if not impossible. Affordable hydrologic models that work well on inland studies simply don't translate to coastal applications. However, more sophisticated supercomputer-based modeling techniques are cost prohibitive.

In a pioneering effort, the St. Johns River Water Management District (SJRWMD) led a team of experts from academia, government, and industry in the development of the Analytical Framework for Coastal and Estuarine Studies (ACES) GIS tool, one of the first comprehensive coastal and estuarine tools. Still under development,

ACES is designed to help scientists accurately monitor and manage the health of a complex estuary from within the Arc Hydro hydrologic environment. [Arc Hydro is a data model template for use with water resources applications that has been developed by Esri in collaboration with key state, national, and international contributors.

Cooperative Development

The research team found that the first step in approaching the river mouth study was to create a GIS-based workbench tool that could incorporate multiple sources. Water in coastal areas often comes from various water sources. This may include surface water flow, incoming tide, artificial waterway, and in some cases groundwater. This tool had to allow virtual estuary generation and bulk parameter estimation.

Facilitate the development and integration of different models in the same framework.

Coastal possibility.

Provided with a GIS-based database of spatial and temporal data describing the environment.

Scientists build a virtual model of the mouth of interest using topography, depth of water, and tidal datum data.

Determine the river mouth bulk parameters (total area, high tide and low tide, volume, depth, tide flow, etc.).

Data related to the flow into and out of the estuary derive more complex parameters such as residence time (time water stays in the system) and flushing potential (the estuary's ability to wash harmful substances).

A survey on the relationship between the water quality and flow rate of the estuary.

Combining traditional observational records and accurate spatial information.

Communicate marine science with GIS.

- G Through GIS, routes and ships could be marked in 3D with a globe.
- G GIS and ship information system monitored data close to real-time.
- Expedition information was delivered to the public through ArcIMS software-based websites.

Ship information system integrated with GIS

In SIS, data collected by scientists on board the ship before integration with GIS could be monitored and visualized.

Navigation data such as location and depth could be confirmed through SIS.

Weather data (temperature, wind, etc.) were recorded, and a water intake system located about 5m below sea level was used to measure salt and water temperature when the ship sailed.

Scientists were able to visualize the data in 2D and table, and the data was automatically related to the GPS point of the SIS.

Combining GIS with SIS opened the opportunity to monitor the quality of the data acquired in near real time, thus making it possible to quickly discover problems, such as sensor malfunctions or activities performed at erroneous locations, and correct them.

Benefits of using GIS.

With the accuracy of GIS technology and its use in Mini-312 Seagrass restoration programs, NOAA has been able to geographically investigate the occurrence of ship ground in FKNMS and collect important data on the size, shape, and amount of damage used in restoration planning and compensation preparation.

With the ability to accurately return to the ground site to perform subsequent evaluations, NOAA can compare the natural recovery status of the site over time.

Modelled recovery forecasts are a means of evaluating the overall success of the program and determining the recovery measures required for each event (if any).

**Visualizing spatiotemporal patterns of city service demand through
a space-time exploratory approach**

JING Changfeng

Beijing University of Civil Engineering and Architecture, China

Green catalysis for the organic contaminated sediment remediation by biochar-based catalysts

Chang-Mao Hung^{1,2}, Chiu-Wen Chen^{1,2}, Cheng-Di Dong^{1,2,*}

ABSTRACT: Aquatic systems are important sinks of persistent organic pollutants (POPs), such as polycyclic aromatic hydrocarbons (PAHs) and phthalate esters (PAEs). Biochar can be produced from many carbonaceous raw biomass, such as agricultural wastes/residues, by pyrolysis or gasification treatment. Recently, there has been an increasing interest in the application of biochar-based catalysts for contaminated sediment remediation due to its highly porous structure, large surface area, and plentiful surface functional sites. This paper provides a review on current green catalysis approach *via* biochar-based catalysts to safeguard environmental health and potential reuse of clean-up sediments as natural resources.

Keywords: Biochar; Catalysis; Organic contaminated; Sediment

1. SEDIMENT CONTAMINATION BY PERSISTENT ORGANIC POLLUTANTS

Persistent organic pollutants (POPs), such as polycyclic aromatic hydrocarbons (PAHs) and phthalate esters (PAEs) are of great concern because of global persistence, which negatively impacts marine ecosystems (Chen et al., 2015; Dong et al., 2017c; 2018a,b; 2019e; 2020b). Sediment is a major ecological health concern, primarily due to its collection of huge number and quantity of hazardous organic chemicals and industrial residues, posing a great risk to the environment and human health (Dong et al., 2015). PAHs and PAEs, because of their hydrophobicity, low water solubility, and high recalcitrance and heterogeneity, have significantly impacted the aquatic environments (Dong et al., 2019b,c; 2020a). Urbanization and industrialization are major sources of environmental POPs that ultimately arrive at sediments and affect adversely the benthic organisms (Hung et al., 2020c; 2021a,b). The bioaccumulation of POPs is known to exhibit teratogenicity and carcinogenicity in exposing animals (Hung et al., 2021d). Therefore, it is imperative to eliminate POPs from the water environment. However, most conventional remediation methods such as biodegradation, composting, coagulation-flocculation, and adsorption only bring about phase transformation of POPs.

2. MANUFACTURE AND CHARACTERISTICS OF BIOCHAR

Biochar (BC) is a carbon-rich material prepared from the pyrolysis of biomass under various conditions (Hung et al., 2020a,b; Pan et al., 2021). Engineered BC has found wide applications in environmental remediation, sustainable agriculture, and energy production owing to its highly porous framework, moisture retention, and pH buffer intensity, in addition to high specific surface area, and abundant oxygen functional species of high metal adsorption capacity (Hung et al., 2021c).

¹ Department of Marine Environmental Engineering, National Kaohsiung University of Science and Technology, Kaohsiung City, Taiwan.

² Sustainable Environment Research Center, National Kaohsiung University of Science and Technology, Kaohsiung City, Taiwan.

* Corresponding author, Department of Marine Environmental Engineering, National Kaohsiung University of Science and Technology, Kaohsiung City, Taiwan, E-mail address: cddong@nkust.edu.tw

Feedstock characteristics and pyrolysis temperature are among the most significant factors properties of BC (Dong et al., 2019f). Recently, BC drew great attention due to its promising potential in environmental control. BC, as an activator of oxidants such as peroxymonosulfate (PMS) to generate reactive oxygen species (ROSs) for environmental remediation, is a typical green catalysis approach toward circular bioeconomy and has roused increasing interests in the field is an ideal alternative to conventional metal-based catalysts that overcome undesirable metal leaching, i.e., a secondary contamination issue (Dong et al., 2017a,b; 2019a,d; Hung et al., 2016a,b; Wang et al., 2021). In summary, value-added carbonaceous materials derived from biomass specifically may be cost-effective and eco-friendly heterogeneous catalyst for the *in-situ* or *ex-situ* remediation of POPs-contaminated sediments.

3. BIOCHAR APPLICATION FOR ORGANIC POLLUTANTS REMEDIATION

Radical-based advanced oxidation processes (AOPs) aided with efficient catalysts can produce highly ROSs. Specifically, activation of peroxides, such as PMS generates sulfate radicals (SR, $\text{SO}_4^{\cdot-}$) and hydroxyl radicals (HR, HO^\bullet), is a powerful means for enhancing the catalytic degradation of recalcitrant POPs (Hung et al., 2021e,f). PMS has been widely studied because of its efficiency and robustness in the complete mineralization of organic chemicals by the abstraction and addition of hydrogen and electron, with the concomitant production of CO_2 , H_2O , and mineral acids (Hung et al., 2021g). With respect to Fenton reagent, PMS-based peroxygen systems have several attributes including high stability over wide pH range, mild reaction conditions, high treatment efficiency, and less toxic products (Hung et al., 2022a). The nature of functional metal-free carbon-rich substances, such as BC, a biomass-derived material, is studied regarding its activation capacity of PMS for the organic contaminated sediment remediation. Overall, the present study significantly expanded knowledge on the metal-free nature of carbocatalysis-boosting BC-based catalysts degradation of POPs (Hung et al., 2022b). In summary, the results illustrated a conceptual model for further understanding the roles of BC on organic contaminated sediment degradation *via* PMS combined with BC-based catalysts (Fig. 1). The BC/PMS system may be useful to realizing the application of green technologies for future water environment bioremediation campaigns.

4. RECOMMENDATION FOR FUTURE

In spite of the existence of fairly extensive literature related to BC application for organic contaminated sediment remediation, the following issues within the subject still remain unsolved:

- (1) The efficiency of POPs degradation depends on the competition kinetics between contaminants, BC, and reactive species in the sediments. Although PMS is a powerful oxidant, it can be catalyzed with various BC to form a more powerful SR. But, there are many challenges to optimize the process, especially for up scaling the applications and the cost-effectiveness.
- (2) A novel promising technique is PMS activated by BC. BC acts as an activator for PMS activation and for remediation of organic contaminated sediment and it is the most environmentally friendly solution, but more research is necessary to further confirm the generation of hazardous by-products.
- (3) What is the optimum dosage of BC-based catalysts during remediation to ensure the best run of the will determine the interaction of BC with organic compounds in sediment?
- (4) The interaction between BC and microbial communities and their symbiotic interaction with sediments, and possibly enhanced degradation efficiency, is not currently understood. Hence, a rigorous definition and sustainability of what a good BC is needs to be established.

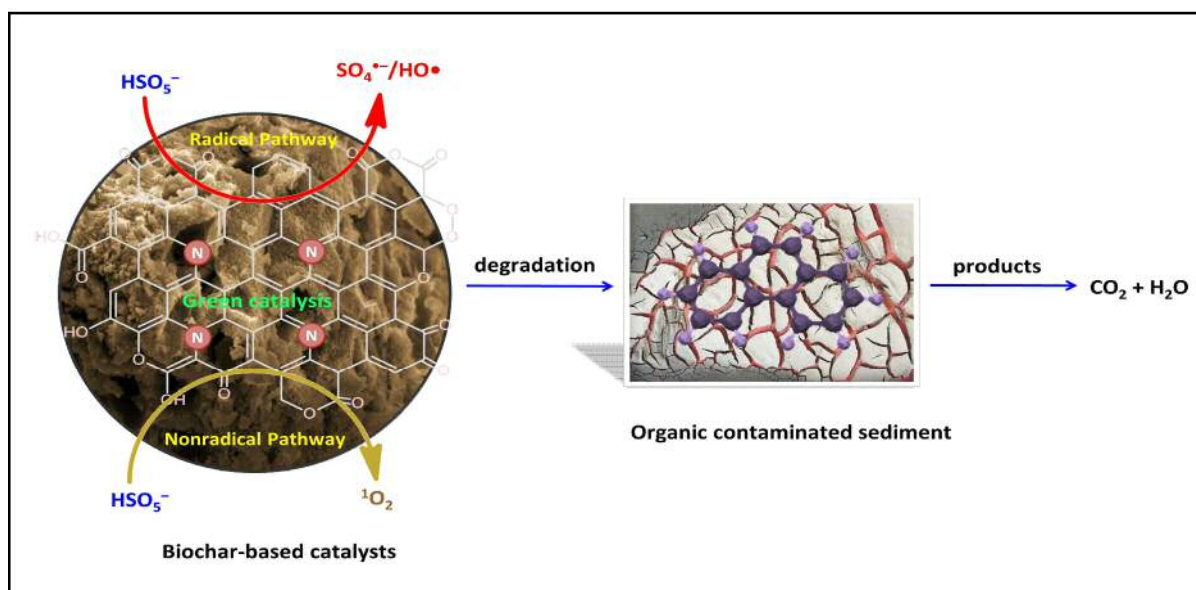


Fig. 1. Concept model of organic contaminated sediment degradation via PMS combined with biochar-based catalysts.

REFERENCES

- [1] Chen, C.W., Nguyen, T.B., Hung, C.M., Chen, C.F., and Dong, C.D., 2015. Removal of polycyclic aromatic hydrocarbons from sediments using chemical oxidation processes. *Journal of Advanced Oxidation Technologies*, vol. 18, pp. 15-22.
- [2] Dong, C.D., Chen, C.W., Chen, C.F., Ju, Y.R., Hung, C.M., and Lou, J.Y., 2015. Environmental monitoring and remediation of the harbor contaminated sediments. *Journal of Ocean and Underwater Technology*, vol. 25, pp. 46-52.
- [3] Dong, C.D., Chen, C.W., and Hung, C.M., 2017a. Preparing carbon-black-coated magnetite nanoparticles: Fabrication, characterization, and heterogeneous persulfate oxidation of methylene blue. *Desalination and Water Treatment*, vol. 63, pp. 357-365.
- [4] Dong, C.D., Tsai, M.L., Chen, C.W., and Hung, C.M., 2017b. Heterogeneous persulfate oxidation of BTEX and MTBE using Fe_3O_4 -CB magnetite composites and the cytotoxicity of degradation products. *International Biodeterioration & Biodegradation*, vol. 124, pp. 109-118.
- [5] Dong, C.D., Chen, C.W., and Hung, C.M., 2017c. Synthesis of magnetic biochar from bamboo biomass to activate persulfate for the removal of polycyclic aromatic hydrocarbons in marine sediments. *Bioresource Technology*, vol. 245, pp. 188-195.
- [6] Dong, C.D., Chen, C.W., Kao, C.M., Chien, C.C., and Hung, C.M., 2018a. Wood-biochar-supported magnetite nanoparticles for remediation of PAH-contaminated estuary sediment. *Catalysts*, vol. 8, pp. 73.
- [7] Dong, C.D., Tsai, M.L., Chen, C.W., and Hung, C.M., 2018b. Remediation and cytotoxicity study of polycyclic-aromatic-hydrocarbon-contaminated marine sediments using synthesized iron oxide-carbon composite. *Environmental Science and Pollution Research*, vol. 25, pp. 5243-5253.
- [8] Dong, C.D., Tsai, M.L., Chen, C.W., and Hung, C.M., 2019a. The efficacy and cytotoxicity of iron oxide-carbon black composites for liquid-phase toluene oxidation by persulfate. *Environmental Science and Pollution Research*, vol. 26, pp. 14786-14796.
- [9] Dong, C.D., Chen, C.W., and Hung, C.M., 2019b. Persulfate activation with rice-husk-based magnetic biochar for degrading PAEs in marine sediments. *Environmental Science and Pollution Research*, vol. 26, pp. 33781-33790.

- [10] Dong, C.D., Lu, Y.C., Chang, J.H., Wang, T.H., Chen, C.W., and Hung, C.M., 2019c. Enhanced persulfate degradation of PAH-contaminated sediments using magnetic carbon microspheres as the catalyst substrate. *Process Safety and Environmental Protection*, vol. 125, pp. 219-227.
- [11] Dong, C.D., Chen, C.W., Tsai, M.L., Chang, J.H., Lyu, S.Y., and Hung, C.M., 2019d. Degradation of 4-nonylphenol in marine sediments by persulfate over magnetically modified biochars. *Bioresource Technology*, vol. 281, pp. 143-148.
- [12] Dong, C.D., Huang, C.P., Nguyen, T.B., Hsiung, C.F., Wu, C.H., Lin, Y.L., Chen, C.W., and Hung, C.M., 2019e. The degradation of phthalate esters in marine sediments by persulfate over iron–cerium oxide catalyst. *Science of the Total Environment*, vol. 696, pp. 133973.
- [13] Dong, C.D., Lung, S.C., Chen, C.W., Lee, J.S., Chen, Y.C., Wang, W.C., Chen, C., Hung, C.M., and Lin, C.H., 2019f. Assessment of the pulmonary toxic potential of nano-tobacco stem-pyrolyzed biochars. *Environmental Science: Nano*, vol. 6, pp. 1527-1535.
- [14] Dong, C.D., Tsai, M.L., Wang, T.H., Chang, J.H., Chen, C.W., and Hung, C.M., 2020a. Removal of polycyclic aromatic hydrocarbon (PAH)-contaminated sediments by persulfate oxidation and determination of degradation product cytotoxicity based on HepG2 and ZF4 cell lines. *Environmental Science and Pollution Research*, vol. 27, pp. 34596-34605.
- [15] Dong, C.D., Chen, C.W., Nguyen, T.B., Huang, C.P., and Hung, C.M., 2020b. Degradation of phthalate esters in marine sediments by persulfate over Fe–Ce/biochar composites. *Chemical Engineering Journal*, vol. 384, pp. 123301.
- [16] Hung, C.M., Chen, C.W., Jhuang, Y.J., and Dong, C.D., 2016a. Fe₃O₄ Magnetic nanoparticles: Characterization and performance exemplified by the degradation of methylene blue in the presence of persulfate. *Journal of Advanced Oxidation Technologies*, vol. 19, pp. 43-51.
- [17] Hung, C.M., Chen, C.W., Liu, Y.Y., and Dong, C.D., 2016b. Decolorization of methylene blue by persulfate activated with FeO magnetic particles. *Water Environment Research*, vol. 88, pp. 675-686.
- [18] Hung, C.M., Huang, C.P., Hsieh, S.L., Tsai, M.L., Chen, C.W., and Dong, C.D., 2020a. Biochar derived from red algae for efficient remediation of 4-nonylphenol from marine sediments, *Chemosphere*, vol. 254, pp. 126919.
- [19] Hung, C.M., Huang, C.P., Chen, C.W., Wu, C.H., Lin, Y.L., and Dong, C.D., 2020b. Activation of percarbonate by water treatment sludge–derived biochar for the remediation of PAH-contaminated sediments, *Environmental Pollution*, vol. 265, pp. 114914.
- [20] Hung, C.M., Huang, C.P., Lam, S.S., Chen, C.W., and Dong, C.D., 2020c. The removal of polycyclic aromatic hydrocarbons (PAHs) from marine sediments using persulfate over a nano-sized iron composite of magnetite and carbon black activator, *Journal of Environmental Chemical Engineering*, vol. 8, pp. 104440.
- [21] Hung, C.M., Huang, C.P., Chen, C.W., Hsieh, S.L., and Dong, C.D., 2021a. Effects of biochar on catalysis treatment of 4-nonylphenol in estuarine sediment and associated microbial community structure, *Environmental Pollution*, vol. 268, pp. 115673.
- [22] Hung, C.M., Huang, C.P., Chen, C.W., and Dong, C.D., 2021b. The degradation of di-(2-ethylhexyl) phthalate, DEHP, in sediments using percarbonate activated by seaweed biochars and its effects on the benthic microbial community, *Journal of Cleaner Production*, vol. 292, pp. 126108.
- [23] Hung, C.M., Huang, C.P., Cheng, J.W., Chen, C.W., and Dong, C.D., 2021c. Production and characterization of a high value-added seaweed-derived biochar: Optimization of pyrolysis conditions and evaluation for sediment treatment, *Journal of Analytical and Applied Pyrolysis*, vol. 155, pp. 105071.
- [24] Hung, C.M., Huang, C.P., Chen, C.W., and Dong, C.D., 2021d. Hydrodynamic cavitation activation of persulfate for the degradation of polycyclic aromatic hydrocarbons in marine sediments, *Environmental Pollution*, vol. 286, pp. 117245.

- [25] Hung, C.M., Huang, C.P., Chen, C.W., and Dong, C.D., 2021e. Degradation of organic contaminants in marine sediments by peroxymonosulfate over LaFeO₃ nanoparticles supported on water caltrop shell-derived biochar and the associated microbial community response, *Journal of Hazardous Materials*, vol. 420, pp. 126553.
- [26] Hung, C.M., Huang, C.P., Chen, C.W., Hsieh, S., and Dong, C.D., 2021f. Remediation of contaminated dredged harbor sediments by combining hydrodynamic cavitation, hydrocyclone, and persulfate oxidation process, *Journal of Hazardous Materials*, vol. 420, pp. 126594.
- [27] Hung, C.M., Huang, C.P., Chen, C.W., and Dong, C.D., 2021g. Activation of peroxymonosulfate by nitrogen-doped carbocatalysts derived from brown algal (*Sargassum duplicatum*) for the degradation of polycyclic aromatic hydrocarbons in marine sediments, *Journal of Environmental Chemical Engineering*, vol. 9, pp. 106420.
- [28] Hung, C.M., Chen, C.W., Huang, C.P., Lam, S.S., and Dong, C.D., 2022a. Peroxymonosulfate activation by a metal-free biochar for sulfonamide antibiotic removal in water and associated bacterial community composition, *Bioresource Technology*, vol. 343, pp. 126082.
- [29] Hung, C.M., Chen, C.W., Huang, C.P., Tsai, M.L., Wu, C.H., Lin, Y.L., Cheng, Y.R., and Dong, C.D., 2022b. Efficacy and cytotoxicity of engineered ferromanganese-bearing sludge-derived biochar for percarbonate-induced phthalate ester degradation, *Journal of Hazardous Materials*, vol. 422, pp. 126922.
- [30] Pan, S.Y., Dong, C.D., Su, J.F., Wang, P.Y., Chen, C.W., Chang, J.S., Kim, H., Huang, C.P., and Hung, C.M., 2021. The role of biochar in regulating the carbon, phosphorus, and nitrogen cycles exemplified by soil systems, *Sustainability*, vol.3, pp. 5612.
- [31] Wang, T.H., Dong, C.D., Lin, J.Y., Chen, C.W., Chang, J.S., Kim, H., Huang, C.P., and Hung, C.M., 2021. Recent advances in carbon dioxide conversion: A circular bioeconomy perspective, *Sustainability*, vol. 13, pp. 6962.

Professor Cheng-Di Dong

Dr. Cheng-Di Dong is a Distinguished Professor at the Department of Marine Environmental Engineering at National Kaohsiung University of Science and Technology (NKUST). He is also the Dean of College of Hydrosphere Science and the Director of Sustainable Environment Research Center (SERC) of NKUST. He earned a Ph.D. degree in Environmental Engineer from University of Delaware in 1993. His current research interests are broadly clustered in the areas of monitoring and remediation of contaminated water, soil and sediments. He is particularly interested in developing fate and transport of contaminants in marine sediments, and remediation of contaminated sediments for the purpose of reuse sediment materials using physical, chemical and biological processes. Prof. Dong has participated in the scientific committee of several conferences and associations and serves as a reviewer in a wide range of international renowned journals. He has published more than 292 papers in leading international journals, 8 patents, 5 book chapters, and edited 8 special issues of scientific journals. He has won 2021 outstanding alumni award of University of Delaware, DE, USA. He was also a Fellow of International Bioprocessing Association.

Compact emergency call to use EOG signal for patient with serious disabilities

Takakazu ISHIMATSU(ishi@nagasaki-u.ac.jp) Nagasaki University
Motohiro TANAKA(tanamo@kurume-it.ac.jp) Kurume Institute Technology

ABSTRACT: In this paper we propose a compact emergency call for patient with serious disability. One typical disease is ALS(Amyotrophic lateral sclerosis). Physical ability of the ALS patient is often limited to eyeball movements. Therefore, eyeball movements are used to communicate with others. While image processing techniques are widely used, the system uses desktop computer and occupies wide space. It is not preferable that devices around patients are big and requires some technique.

Proposed emergency call is simple and compact. It doesn't violate nursing environments around patients. One more feature of the system is that simple configuration means the emergency call is tough in the nursing conditions. We applied the emergency call to an ALS patient. The result was satisfactory.

1. Introduction

Patients suffering intractable disease like ALS and muscular dystrophy have difficulty to move their muscles intentionally. Since their muscular abilities deteriorate, their physical movements of limbs and mouth are limited. It should be noted that their communication abilities with friends and family members often become difficult in couples of years. Some patients can move only his eyeball. For such patients in serious difficult situation, eye tracking technique to detect gaze direction are often employed as an efficient communication input device for communication and environmental control system. One typical communication system is shown in Fig.1, where the patient can control communication system and control electric appliances using eye-tracking system. The eye tracking system detects gaze direction by using the image processing of patient's eyeball.

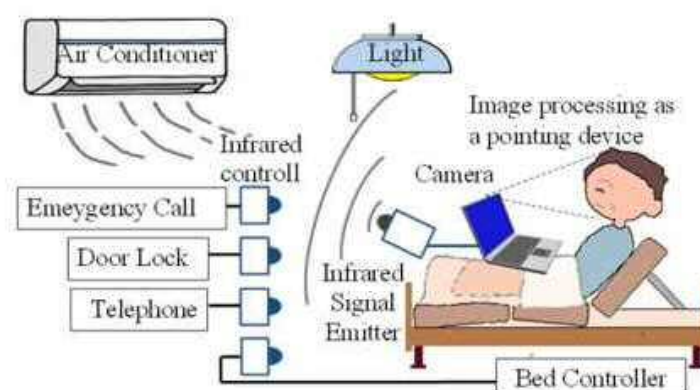


Fig. 2 Configuration of life support system.

Eye tracking techniques are applicable into various fields, medical, industry, amusement and so on. Communication devices for patients to use image processing are commercially available. Therefore, patients with serious muscular abilities often use these communication systems supported by the medical insurance service.

As another technique to detect gaze direction, EOG (Electro_oculogram) is focused. EOG can be obtained by measuring the differential voltage between the left and right temples. The EOG reveals the gaze direction based on the physical phenomena that between the front side of the eyeball have electrically positive potential. And the rear side of the eyeball have electrically negative potential.

Therefore, if you move your eyes rightward, on your right temple positive electric potential can be detected. The electric voltage difference between both temples can be obtained by electric devices. Since the voltage difference between the temples is less than one mv, high precision sensor is required.

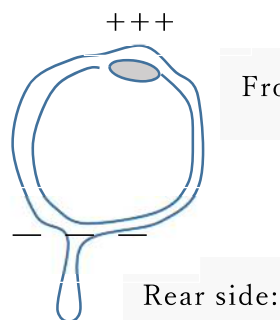


Fig.2 Eyeball potential

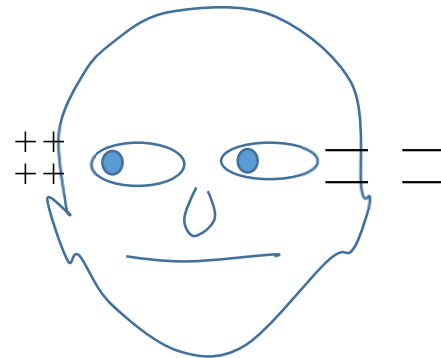


Fig.3 EOG around temples

Already the EOG sensor is commercially available. The EOG sensor is used as an interface devices and also a clinical device to estimate physical condition during sports and driving and also some other tasks.

One feature of EOG sensor is that the sensor can be compactly achieved by using a one-tip computer and high precision AD converter.

We applied the EOG sensor to an emergency call, since the emergency call can be readily achieved in a compact body by using EOG sensor.

In this paper we propose a compact emergency call using EOG signals.

2. Configuration of proposed emergency call using EOG signals.

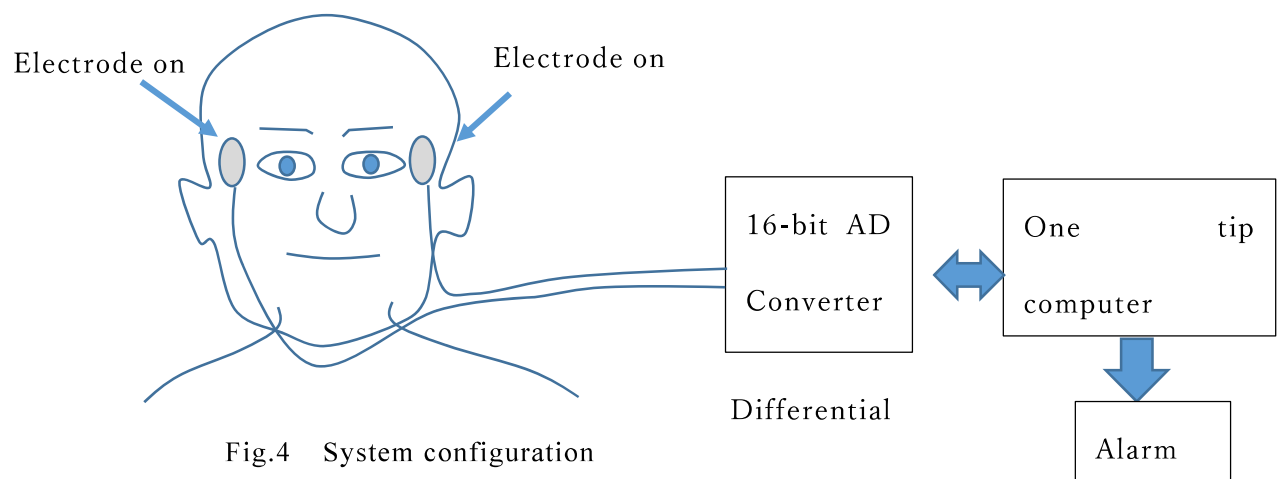


Fig.4 System configuration

We propose a compact emergency call to use EOG signal as shown Fig.4. This emergency call is designed to enable a ALS patient to control the alarm signal by moving his eyeball. His remaining physical ability is limited to move eyeball. He requested a compact emergency call with simple operations.

Proposed emergency call could be readily achieved using one-tip computer(Arduino Nano) and high precision16-bit AD converter(ADS1115). Using this high precision AD converter, the emergency call does not require any analog amplifier and analog data processing. Filtering and smoothing on the data can be executed by the software. The proposed system is revealed in Fig.5. On the main board one-tip computer (Ardiono nano) and 16bit AD converter(ADS1115) are mounted.

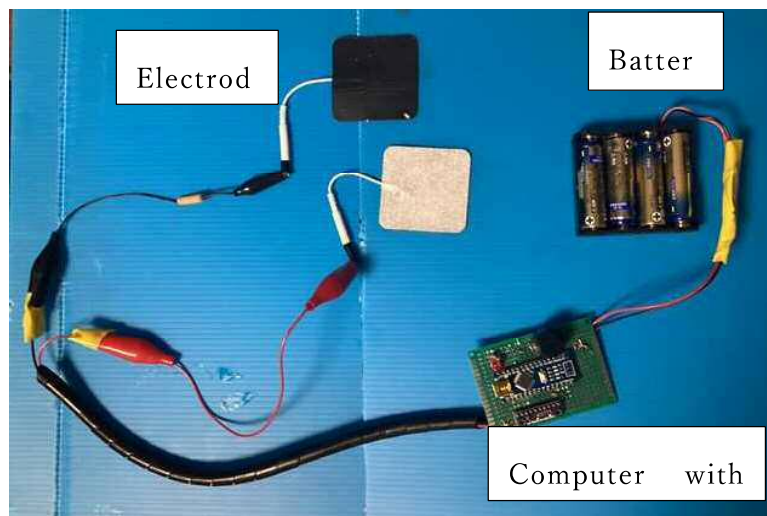


Fig. 5 Compact configuration of the emergency call

3. Data processing of the proposed sensor

Gaze direction can be obtained by the Program shown in Fig. 6.

Firstly, EOG signals are obtained 38 times at differential electrical voltage between temples via AD converter. And by averaging 38 data the i -th EOG estimated data $Av(i)$ is obtained. Furthermore, a smoothing filter

$$Sf(i) = Sf(i-1) \times 0.98 + Av(i) \times 0.02$$

is employed, where $Sf(i)$ is the i -th output of smoothing filter.

EOG signal is affected by the condition and clinical condition as well.

In Fig.7, averaged EOG signal $Av(i)$ and output $Sf(i)$ of smoothing filter are shown.

At the beginning region, we mounted electrodes on the patient's temples. Therefore, you can find remarkable changes of averaged EOG signal. But after 20 seconds the output of smoothing filter approaches to averaged EOG signals. Even if the averaged EOG changes big, the output of the smoothing filter tries to keep smooth.

Comparing the averaged EOG signal and output of smoothing filter, EOG signal changes caused by gaze direction change can be estimated.

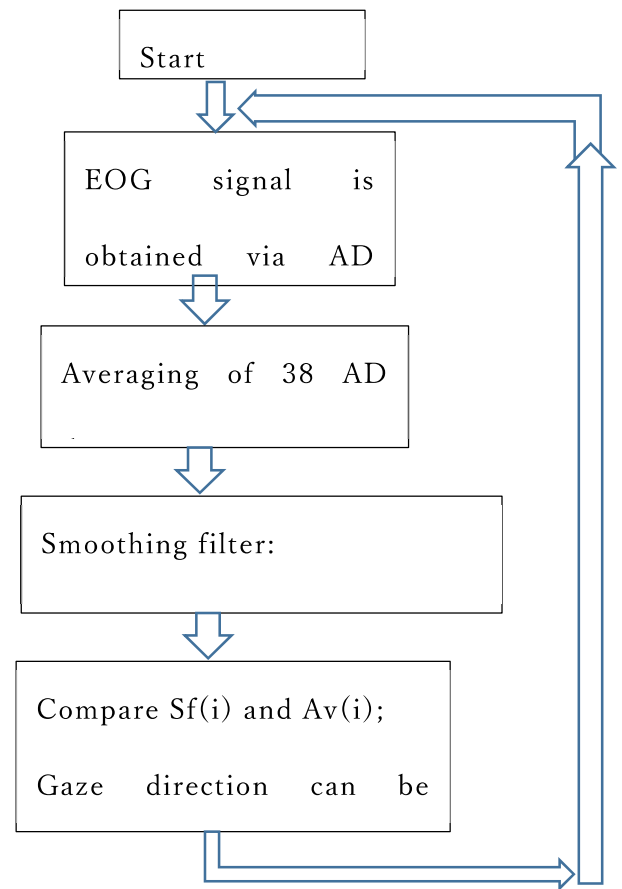


Fig.6 Flow of data

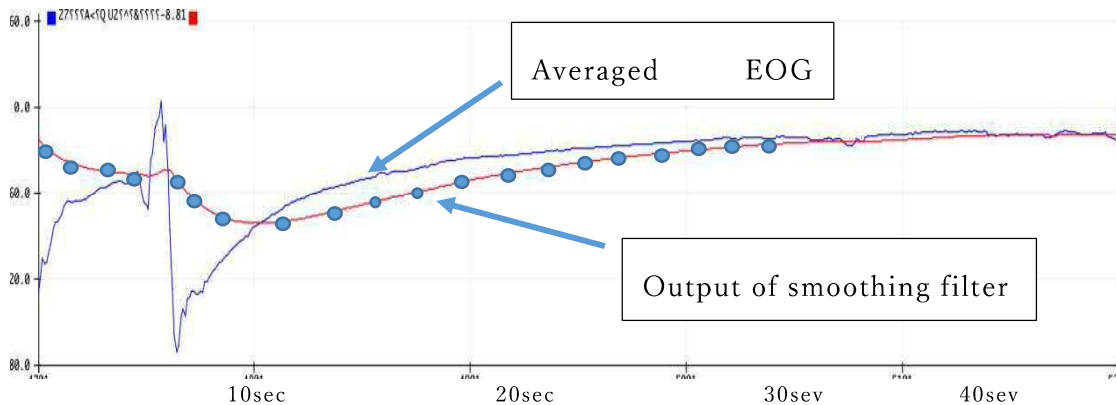


Fig.7 Averaged EOG signal and output smoothing filter

4. Experiments

Experiments were conducted by a student.

He repeated to move eyes 30 degrees to the left direction and move 30 degrees next to the right direction. During this experiment he is requested to fix his head. Same experiments were also conducted with 20 degrees to the left and right directions.

The EOG signal obtained are shown in Fig.8.

Comparing the EOG signal with smoothing data, eyeball movements can be easily detected

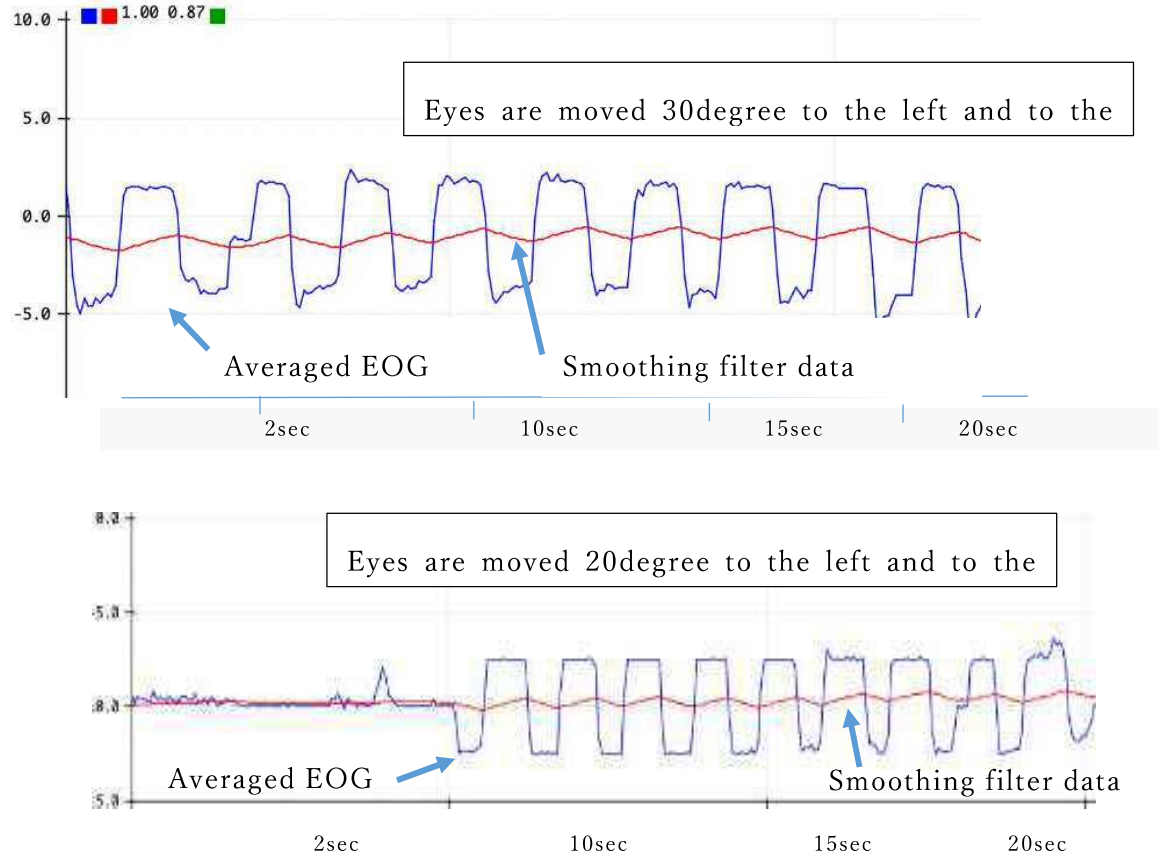


Fig.8 Eyeball movements and EOG signals

These data show that proposed emergency call can detect the eyeball movement accurately.

We applied this emergency call to an ALS patient. His physical ability is limited to eyeball movements as shown in Fig.9.



5. Conclusions

We proposed a compact emergency call to use EOG signals for people with seriously disabled. One distinguished feature of the system is that the emergency call to use eyeball movements can be achieved with simple configuration. One-tip computer and an AD converter module are enough to build the emergency call. Since analog amplifiers are not required, all the required process can be realized by the programming. Proposed emergency call was satisfactory to the patient and the care giver. We are now trying to help people with serious disability using EOG signal device.

References

1. Chao Zhang, Haruo Nakashima, Motohiro Tanaka et al,"Computerized environment for People with serious disability, 2012 Fifth International Conference on Intelligent Networks and Intelligent Systems,
2. Tohru YAGI, Atsuko MIYANAGA et al, A Study on an Eye-gaze Interface using EOG, https://www.jstage.jst.go.jp/article/lifesupport1996/18/Supplement/18_Supplement_93/_pdf
3. Tomotaka USUI, Takumi BAN, Toshiyuki YAMAMOTO, A Study on Estimating Eye Direction using Smart Eyewear, Symposium DICOMO2016 , pp.1172-1174,2016
4. Chao Zhang, Dr.thesis tytled" Vision-Based Displacement Sensor for People with Serious Spinal Cord Injury, Nagasaki Univerity,2016.

Sessions

Modeling and Simulation of Rainfall Effect of Autonomous Driving LiDAR Sensor

TaeYeon Park^{*}, Jangwoo Cheon^{**}, Impyeong Lee^{***}

ABSTRACT: Recently, autonomous driving simulators capable of building various environments and scenarios have been widely used for driving experiments and safety verification of autonomous vehicles. But while the adverse weather influence the performance of automotive LiDAR sensor, there have been few studies that physically reflect these weather effects on autonomous driving simulators. In this work, LiDAR radiometric modeling is performed reflecting the effect of real rainfall in LiDAR sensor. Finally, the developed model is applied to the simulator and the generated simulation data is compared with the real data to perform evaluation and verification of this model.

Keywords¹: LiDAR Sensor Modeling; Radiometric Model; LiDAR Simulation

1. Introduction

Recently, with the technological development of autonomous vehicles, the market for autonomous vehicles is expanding, and attention is also focused on safety of vehicles. Autonomous vehicles drive while recognizing, determining, and controlling based on sensors mounted. Representative cognitive sensors are camera, lidar and radar. Among them, the LiDAR is a sensor that emits a laser pulse and calculates the distance, speed and direction to the surface by measuring the time and intensity of light returning from the reflected surface, and is one of the representative sensor in autonomous vehicle. However, there are limitations to these LiDAR sensors. Since it emits laser pulse to the air, it has the disadvantage of being relatively vulnerable to adverse weather. Therefore, a driving test of an autonomous vehicle under adverse weather is essential.

The most realistic driving test method is the Field Test. However, it is difficult to conduct repetitive experiments in various scenarios and environments. So autonomous driving simulators that are safe and can build various scenarios and environments are widely used to overcome this. But studies on simulators that physically reflect the weather effect are insufficient.

LGSVL is an autonomous driving simulator that is widely used and can be simulated in various weather environments. However, although the visual effect on the camera is only considered, not LiDAR. [1] performed the LiDAR radiometric modeling based basic LiDAR equation for physically reflecting the effect on rainfall on the simulator. However, this model requires detailed specifications for the LiDAR, making it difficult to model.

^{*} University of Seoul, siam33@uos.ac.kr

^{**} ^{*} Corresponding author, University of Seoul, iplee@uos.ac.kr

^{**} University of Seoul, khai0614@uos.ac.kr

Thus, in this study, the effect of the real rainfall environment on the LiDAR is identified, and a LiDAR radiometric model that can physically reflect these effect in simulation is developed. In addition, the developed model is applied to the simulation to generate simulation data. This is compared with the real LiDAR data to verify the accuracy of this model. The effect on LiDAR sensor in real rainfall environments typically has a signal attenuation effect from atmospheric transmission of laser pulse and noise effect caused by collisions between laser and raindrop particles [2]. In this work, radiometric modeling is performed on the LiDAR signal attenuation effect.

2. Methodology

LiDAR simulation requires a virtual environment model and a LiDAR sensor model defined for the LiDAR operation method. Therefore, in this study, a simulation scene for performing simulation is constructed and a LiDAR radiometric model suitable for the operation method of the LiDAR sensor is developed. This model is verified based on real data acquired in real rainfall environment.

2.1 Validation Dataset Acquisition

In this study, data in real rainfall environment was acquired to verify the developed model. Data were acquired using the Velodyne VLP-16 LiDAR sensor in the parking lot of University of Seoul. In order to evaluate the degree of attenuation of the intensity by precipitation for objects frequently encountered by the vehicle on the road, a vehicle and road cones were arranged as shown in Figure 1 in a parking lot composed of asphalt surface to obtain data.

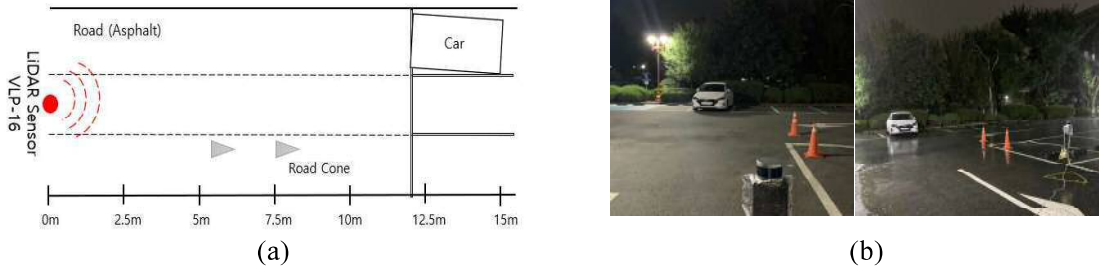


Figure 1. (a) Experimental environment drawing (b) Real experiment environment

2.2 Simulation Scene Construction

A virtual environment model is required to perform the LiDAR simulation. In this study, the developed model is verified based on the real data. Therefore, a simulation scene is constructed similar to the real experimental environment. The Simulation scene was constructed as shown in Figure 2(a) using the Matlab RoadRunner program. In addition, a simulation environment is constructed by defining the reflectivity value of the real medium for each object.

2.3 Radiometric Modeling

LiDAR sensor has a lot of attenuation caused by the surrounding environment while the laser pulse is reflected back to the target, which is called a LiDAR radiometric model.[3].

$$Pr = \frac{P_t D_f^2 \eta_{sys} \eta_{atm} \rho \cos \theta}{4r^2} \quad (1)$$

Where, P_r is the received power, P_t is the transferred power, D is the receiver aperture diameter, η_{sys} is the system transmission factor, η_{atm} is the atmospheric transmission factor and expressed as $e^{-2\alpha r}$, α is a scattering coefficient, a measure of the ability of particles to scatter photons out of a beam of light, ρ is reflectance, θ is angle of incidence, and r is the range. Here, the Eq. (1) can be simplified as shown in Eq. (2) under the assumption that the surrounding environment remains unchanged and the weather is clear using the same LiDAR sensor [4]. Assuming that the weather is clear, α can be assumed to be 0, and the atmospheric transmission factor is calculated to be 1.

$$I \propto P_r \propto \frac{\rho \cos \theta}{r^2} \quad (2)$$

However, as a result of comparing the intensity derived based on the radiometric model in Eq. (2) with the real LiDAR intensity, it can be confirmed that the measured intensity is not modeled according to the corresponding equation [5]. Therefore, in this study, as shown in [6], the distance effect on the intensity is modeled using a polynomial function. In [6], modeling is performed without considering the weather, and the atmospheric transmission factor is 1. However, since this study reflects the attenuation effect on the rainfall environment, the model in [6] can be expressed as Eq. (3).

$$I = \rho \cos \theta f(r) e^{-2\alpha r} \quad (3)$$

$$\alpha = \frac{\pi}{4} \int_{D=0}^{\infty} D^2 Q_{EXT}(D) N(D) dD \quad (4)$$

$f(r)$ is a polynomial function representing the distance effect, and the scattering coefficient α can be calculated as shown in Eq. (4) based on the Mie theory. D represents the diameter of droplets, Q_{EXT} is efficiency coefficient, $N(D)$ is Drop Size Distribution, which represents the total number of droplets per unit volume, and we used Marshall Palmer Distribution.

2.3 Simulation

In this study, LiDAR simulation in a rainfall environment is performed using Unity Game Engine. Simulation data were generated using the Constructed simulation environment and the developed signal attenuation model, and precipitation was classified into 5 types (6, 18, 30, 48, 60 [mm/h]) and the experiment was conducted.

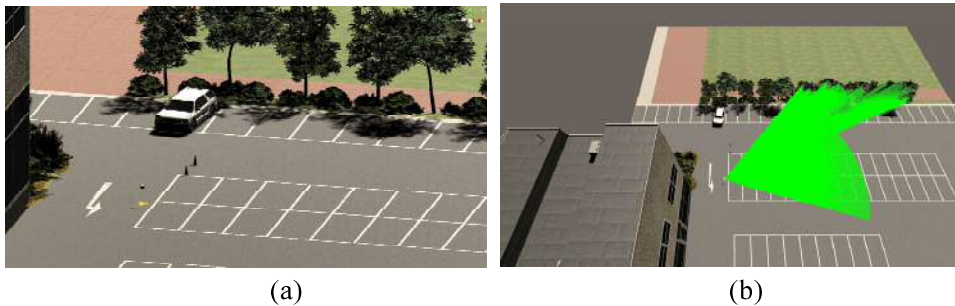


Figure 2. (a) Simulation Scene in Unity, (b) LiDAR operation scene in Simulation

3. Results and Discussion

In this study, the accuracy of simulation data is evaluated based on the real LiDAR data. The average intensity per precipitation is calculated by segmenting the vehicle and asphalt ($15m^2$) and the difference in intensity between the real data and simulation data is analyzed. Figure 3 is a graph showing the average intensity of each target of measurement and simulation. On average, there was a difference about 0.407DN for asphalt, and the smallest difference of about 0.023DN for 18mm/h. In the case of vehicles, there was a difference of about 0.712DN and the smallest difference of about 0.143DN for 48mm/h. In this study, the distance effect on the real intensity was considered, and more similar results to the real data could be derived by adding the reflective value of the real object medium. In addition, it can be seen that the atmospheric transmission factor is applied to the model based on Mie theory, and despite the change in precipitation, there is no significant difference from the real data.

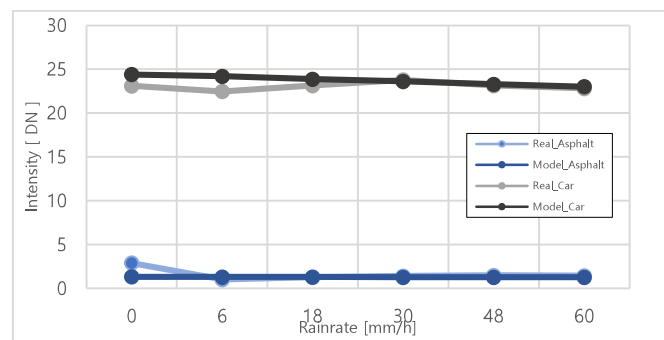


Figure 3. Real data and simulation data results for each target

4. Conclusion

In this study, the effect of actual rainfall on the LiDAR sensor was modeled so that the rainfall effect could be physically reflected on the autonomous driving simulator, and this was compared and evaluated with real data. As a result, there was not much difference from the real data for the vehicle and asphalt. In the future, if the modeling of the noise effect as well as the signal attenuation effect is performed, it is believed that LiDAR simulation for more realistic rainfall will be possible.

Acknowledgement

This research was supported by the Institute of Information & Communication Technology Planning & Evaluation (IITP) funded by the Ministry of Science, ICT & Future Planning. (No. 2019-0-00399, Development of SW technology for recognition, judgement and path control algorithm verification simulation and dataset generation.).

References

- 1) R. H. Rasshofer, M. Spies, and H. Spies, "Influences of weather phenomena on automotive laser radar systems," Adv. Radio Sci., vol. 9, pp. 49–60, 2011.

- 2) K. Yoneda, N. Suganuma, R. Yanase, and M. Aldibaja, “Automated driving recognition technologies for adverse weather conditions,” *IATSS Res.*, vol. 43, no. 4, pp. 253–262, Dec. 2019.
- 3) Wagner, W., 2010, Radiometric calibration of small-footprint full-waveform airborne laser scanner measurements: basic physical concepts, *ISPRS Journal of Photogrammetry and Remote Sensing*, Vol. 65, No. 6, pp. 505-513
- 4) Carrea, D., Abellan, A., Humair, F., Matasci, B., Derron, M. H., and Jaboyedoff, M., 2016, Correction of terrestrial LiDAR intensity channel using oren–nayar reflectance model: an application to lithological differentiation, *ISPRS Journal of Photogrammetry and Remote Sensing*, Vol. 113, pp. 17-29.
- 5) S. Kaasalainen, A. Jaakkola, M. Kaasalainen, A. Krooks, and A. Kukko, “Analysis of incidence angle and distance effects on terrestrial laser scanner intensity: Search for correction methods,” *Remote Sens.*, vol. 3, no. 10, pp. 2207–2221, 2011.
- 6) Gyuseok Lee, Impyeong Lee, “Precise Modeling of LiDAR sensors for Autonomous Driving Simulators”, Master thesis, Department of GeoInformatics Engineering University of Seoul, 2021

The supports for the older people living in the community provided by PHNs and CWSs of Community Comprehensive Support Centers in Kyushu, Japan during the COVID-19 pandemic.

Ryoko Kawasaki¹⁾, ○Yuka Kawabata²⁾, Rieko Nakao¹⁾ Ohnishi Mayumi²⁾

1) Graduate School of Biomedical Sciences, Nagasaki University

2) Department of Public Health Nursing, Health Sciences (Master Course), Graduate School of Biomedical Sciences, Nagasaki University

Introduction

Community Comprehensive Support Centers (CCSCs) are small neighborhood-based support centers for the older people. There are 5221 CCSCs in Japan, with 580 in the Kyushu area (excluding Okinawa Prefecture)¹⁾. The CCSC is a regional support center for the elderly living in the community that provide support services in four areas: comprehensive and continuous care management, care management for prevention of being cared, comprehensive consulting, and rights protection²⁾. The CCSC is staffed by public health nurses (PHNs) – including nurses who have experience working in the community, certified social workers (CSWs), and nursing care specialists. Of these, PHNs and CSWs are nationally certified.

While the COVID-19 pandemic changed everyone's lifestyles dramatically, the older adult population was found to be particularly vulnerable. The World Health Organization (WHO, 2020) suggested that older adults, particularly those isolated or in cognitive decline – may become more anxious, angry, stressed, agitated, and withdrawn while in quarantine³⁾.

The purpose of this study is to determine the changes in the frequency of face-to-face and online support given by PHNs and CSWs of CCSCs to the older people in the community during the COVID-19 pandemic when social distancing was required. In addition, we will identify the assessment items for the older people that CCSC PHNs and CSWs found particularly challenging due to the decrease in face-to-face support.

Methods

1. Participants

Study participants were PHNs and CSWs working in each of the 558 CCSCs located in seven prefectures in the Kyushu area (excluding Okinawa Prefecture) of Japan. There were a total of 1116 study participants – one PHN and one CSW from each CCSC.

The study period was from 26th August to 7th October, 2021, covering the period when the number of new infections per day exceeded 25,000 in Japan and local governments were

actively calling for people to refrain from traveling outside the prefecture and wearing face masks when eating out⁴⁾.

2. Data collection

This is a cross-sectional study based on a self-administered questionnaire survey conducted by mail. This study was approved by Ethics Committee of Nagasaki University Graduate School of Biomedical Sciences. In addition, there is no conflict of interest in this study.

3. Study items

The study items were the participant's profession, sex, age, years of experience in CCSC, change in frequency of face-to-face and online work after the COVID-19 pandemic ("decreased", "remained the same", or "increased" compared to before the pandemic), and perceived difficulties in assessing the older people for the six assessment items ("very difficult", "somewhat difficult", "neither difficult nor not difficult", "not very difficult", and "not difficult"). The assessment items for the older people consisted of: 1) planning of long-term care prevention services, 2) needs assessment for long-term care prevention, 3) determination of urgency of needs, 4) prioritization of nursing care services, 5) setting of care goals, and 6) determining the necessity of introducing new services.

4. Analytical method

Descriptive statistics of each question item were calculated. The responses to difficulties in assessment of the older people for the six assessment items were divided into three categories: "very difficult/somewhat difficult", "neither difficult nor not difficult" and "not very difficult/not difficult", and a chi-square test or Fisher's exact test were conducted to determine the relationship between changes in frequency of face-to-face and online work after the COVID-19 pandemic. SPSS ver.28 was used for the analysis and the statistical significance level was less than 5%.

Results

A total of 452 respondents returned the questionnaire (response rate 38.5%), of which 373 (181 PHNs and 192 CWSs) were used for the analysis, excluding those who did not indicate their occupation and those with less than 3 years of experience (valid response rate: 31.8%). Of the 373 respondents, 284 (76.1%) were female, and the largest age group was in their 40s (133; 35.7%), followed by those in their 30s (116; 31.1%). The mean number of years of experience in the CCSC was 6.6 years (SD 3.1).

One hundred and ninety-six respondents (52.5%) reported a decrease in face-to-face work after the pandemic, 149 (39.9%) reported that the amount of face-to face work did not change compared to before the pandemic, and 28 (7.5%) reported an increase compared to before the pandemic. The group that reported less face-to-face work than before the COVID-19 pandemic was significantly more likely to report difficulties in planning of long-term care prevention services ($P=0.028$), needs assessment for long-term care prevention ($P<0.001$),

and determination of urgency of needs ($P<0.001$) than the group that reported the same frequency or an increase in frequency.

On the other hand, 155 respondents (30.8%) reported that their online (e.g. video conferencing system) work increased after the pandemic, while 255 respondents (68.4%) reported that their amount of online work decreased or remained the same as before the pandemic. The group that reported an increase in online work compared to before the COVID-19 pandemic was significantly more likely to report difficulties in needs assessment for long-term care prevention ($P=0.002$), determination of urgency of needs ($P=0.011$), and prioritization of nursing care services ($P=0.007$) than the group that reported the same frequency or a decrease in online work.

Discussions & Conclusion

Although needs assessment and urgency judgment of the older people require highly specialized professional skills, it was found that social distancing associated with the COVID-19 pandemic increased the degree of difficulty for such professionals, in this case PHNs and CSWs. On the other hand, online work by CCSC professionals increased during the pandemic, but difficulties in assessing the needs of the older people through online work also became apparent. The introduction of ICT into the community health care system is planned to be further developed in the future⁵⁾, and PHNs and CSWs are urgently required to be trained in ICT-based needs assessment for the older people.

Table. 1

Characteristic of the respondents		N=373	
		n	%
Sex	Female	284	76.1
	Male	85	22.8
Age	20's	17	4.6
	30's	116	31.1
	40's	133	35.7
	50's	81	21.7
	60's and over	23	6.2
Profession	PHN	181	48.5
	CSW	192	51.5
Years of experience in CCSC (mean)		6.6	(SD=3.1)
Change in frequency of face-to-face work after the COVID-19 pandemic			
	Decreased	196	52.5
	Remained the same	149	39.9
	Increased	28	7.5
Change in frequency of online work after the COVID-19 pandemic			
	Decreased or Remained the same	255	68.4
	Increased	115	30.8

Table2.

Relationship between assessments for the older people that CCSC PHNs and CSWs found difficult after the COVID-19 pandemic and changes in the frequency of face-to-face work

very difficult/somewhat difficult assessment items for the older people	face-to-face work						P-value
	Decreased		Remained the same		Increased		
	n	%	n	%	n	%	
1) planning of long-term care prevention services	74	38.3	33	22.3	7	25.0	0.028
2) needs assessment for long-term care prevention	115	59.3	45	30.2	13	46.4	<0.001
3) determination of urgency of needs	92	47.7	38	25.7	5	18.5	<0.001
4) prioritization of nursing care services	71	36.8	44	29.5	4	14.3	0.139
5) setting of care goals	79	40.9	43	29.1	12	42.9	0.159
6) determining the necessity of introducing new services	109	56.5	69	47.6	13	46.4	0.088

chi-square test or Fisher's exact test

References

- 1) Ministry of Health, Labor and Welfare of Japan.
https://www.mhlw.go.jp/stf/seisakunitsuite/bunya/hukushi_kaigo/kaigo_koureisha/chiiki-houkatsu/. (Access confirmed on Nov 23, 2021.)
- 2) Ministry of Health, Labor and Welfare of Japan. Establishing 'the Community-based Integrated Care System' 2017. https://www.mhlw.go.jp/english/policy/care-welfare/care-welfare-elderly/dl/establish_e.pdf (Access confirmed on Nov 23, 2021.)
- 3) World Health Organization. Mental health and psychosocial considerations during the COVID-19 outbreak. 2020.
<https://www.who.int/docs/default-source/coronaviruse/mental-health-considerations>
(Access confirmed on Nov 23, 2021.)
- 4) Countermeasures for COVID-19 infection. Cabinet Secretariat of Japan. (Japanese)
<https://corona.go.jp/emergency/> (Access confirmed on Nov 23, 2021.)
- 5) Ministry of Internal Affairs and Communications of Japan. The 2020 White Paper on Information and Communications in Japan.
https://www.soumu.go.jp/main_sosiki/joho_tsusin/eng/whitepaper/2020/index.html .
(Access confirmed on Nov 23, 2021.)

Analysis of Positioning Accuracy of GNSS RTK System according to Positioning Environment

Jae-Cheol Lee ^{*}, Dong-Ha Lee ^{**}

ABSTRACT: For the realization of smart land, the user base for GNSS-based positioning data increases with the completion of the advancement of the satellite reference point infrastructure due to the development of GNSS positioning technology, and accordingly, it is necessary to improve the accuracy of GNSS-based precise positioning performance in various positioning environments. Therefore, in this study, precision positioning (kinematic positioning) accuracy analysis for performing field-specific GNSS-based high-precision positioning using satellite navigation technology and broadcasting communication technology for positioning accuracy analysis of the GNSS RTK system according to the positioning environment of the GNSS RTK system. For this purpose, after selecting an available reference point in the field, the GNSS reception environment was analyzed (static positioning). After that, the vehicle was equipped with GNSS positioning equipment to perform precise positioning. Four types of positioning methods (Post Kinematic, Single RTK, VRS, MBC B'RTK) were used to perform GNSS movement status positioning. As a result of this study, it was confirmed that there was no significant difference in the precision of the three methods of Single RTK, VRS, and MBC B'RTK based on Post Kinematic, and GNSS RTK for each construction site was confirmed by ensuring excellent accuracy.

Keywords: GNSS RTK System¹; Static positioning; Kinematic Positioning; Accuracy

1. Introduction

For the realization of smart land, the user base for GNSS-based positioning data increases with the completion of the advancement of the satellite reference point infrastructure due to the development of GNSS positioning technology, and accordingly, it is necessary to improve the accuracy of GNSS-based precise positioning performance in various positioning environments. Therefore, in this study, precision positioning (kinematic positioning) accuracy analysis for performing field-specific GNSS-based high-precision positioning using satellite

^{*} Department of Integrated Energy and Infra System, Kangwon National University, Korea, essentialee@kangwon.ac.kr

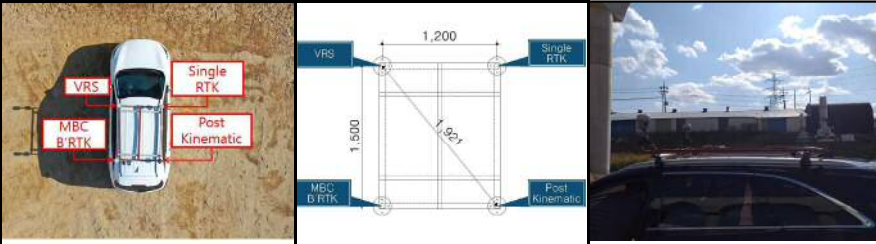
^{*} Corresponding author, Department of Civil Engineering, Kangwon National University, Korea, geodesy@kangwon.ac.kr

navigation technology and broadcasting communication technology for positioning accuracy analysis of the GNSS RTK system according to the positioning environment of the GNSS RTK system. For this purpose, after selecting an available reference point in the field, the GNSS reception environment was analyzed (static positioning). After that, the vehicle was equipped with GNSS positioning equipment to perform precise positioning. Four types of positioning methods (Post Kinematic, Single RTK, VRS, MBC B'RTK) were used to perform GNSS kinematic positioning.

2. Experimental Section

In order to analyze the positioning accuracy of the GNSS RTK system according to the positioning environment, the vehicle was equipped with GNSS survey equipment and precise positioning (kinematic positioning) was performed. Post Kinematic, Single RTK, VRS, MBC B'RTK GNSS kinematic positioning was performed, the reception interval was set to 1 second, and the vehicle was driven at low speed (15 to 30 km/h) to match the conditions as much as possible with the field work vehicle. It was. The outline of GNSS RTK positioning is shown in Table 1.

Table 1. GNSS RTK positioning (kinematic positioning) overview

Purpose	After acquiring MBC B'RTK, VRS, Single RTK, Post-Kinematic data using the moving state method, analysis of MBC B'RTK moving state positioning performance through mutual GNSS RTK moving state positioning quality analysis			
Positioning Method	Kinematic positioning			
	Post Kinematic	Single RTK	VRS	MBC B'RTK
Observation Time	6 hours			
GNSS Reception Time	1 second			
Kinematic Positioning Holder Concept Diagram and Photo				

3. Results and Discussion

Post Kinematic, Single RTK, VRS, and MBC B'RTK data acquired by performing GNSS RTK kinematic positioning within the study area were processed and analyzed using the RTKLib baseline analysis program. Among the measurement methods, the Post Kinematic

value had the highest accuracy, so the TM coordinate values of the Post Kinematic method and other methods were used and compared with the base line length of the cradle used in the study. The graph of the baseline length deviation from the processed data value and the data analysis results are shown in the Table 2, 3.

Table 2. GNSS RTK positioning data baseline length deviation graph

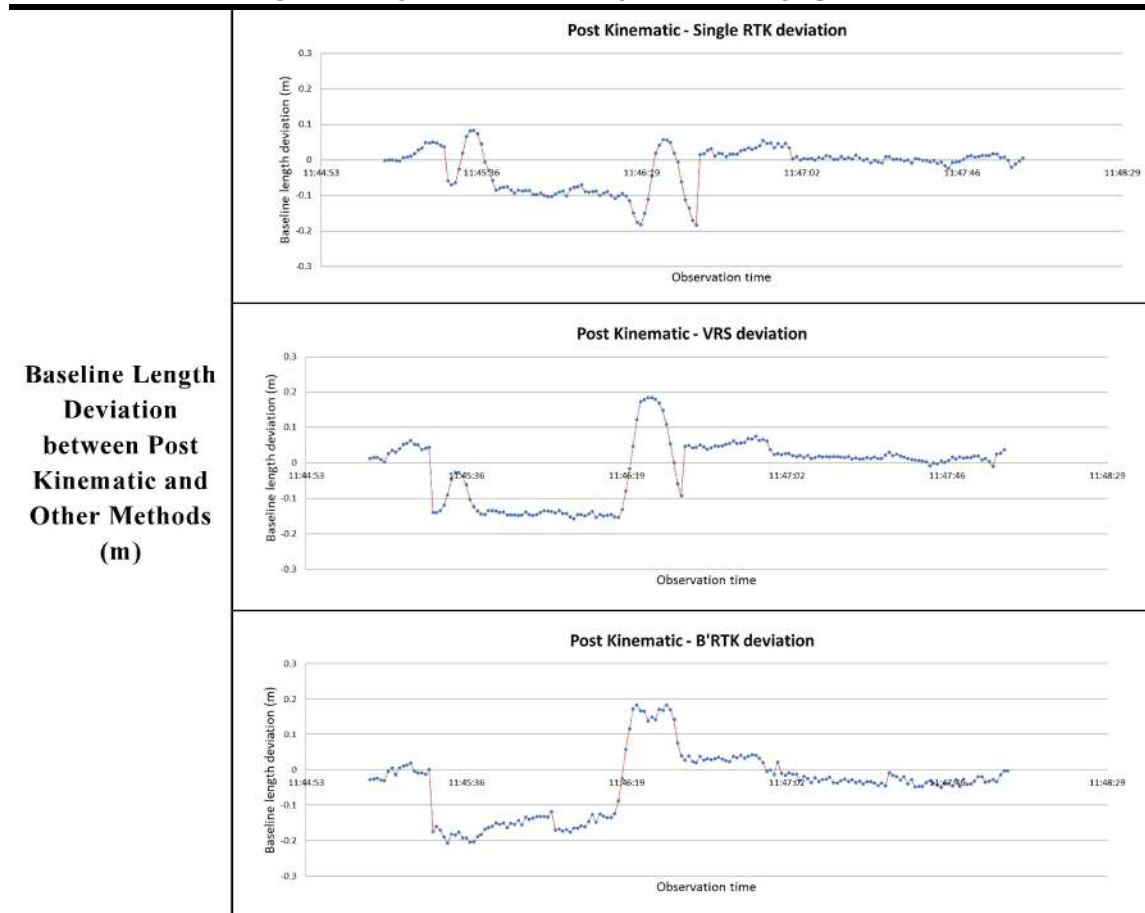


Table 3. GNSS RTK positioning (kinematic positioning) data analysis result

Baseline Length Deviation between Post Kinematic and Other Methods (m)		Single RTK (1.2m)	VRS (1.5m)	MBC B'RTK (1.92m)
	Average Baseline Length	1.24157	1.52025	1.93763
	Maximum Deviation	0.08235	0.18251	0.18436
	Minimum Deviation	-0.18495	-0.15787	-0.20795
	Mean Deviation	-0.02026	-0.01670	-0.04158
	Standard Deviation	±0.05744	±0.08613	±0.09173

4. Conclusion

As a result of the final processed data, the standard deviation of the baseline length between Post Kinematic and Single RTK is ± 0.05744 m, the standard deviation of the baseline length between Post Kinematic and VRS is ± 0.08613 m, and the standard deviation of the baseline length between Post Kinematic and MBC B'RTK is ± 0.05744 m. It was found to be ± 0.09173 m.

Therefore, it was confirmed that there was no significant difference in the standard deviation of the baseline length for the three methods of Single RTK, VRS, and MBC B'RTK based on Post Kinematic, and it was confirmed that excellent accuracy was secured.

References

- 1) Yun, H., Lee, D., Lee, Y. and Cho, J., 2006, Development of GPS Data Quality Control Program, Journal of the Korean Society of Surveying, Geodesy, Photogrammetry and Cartography 24(1), pp. 9-18.
- 2) No, S., Han, J. and Kwon, J., 2012, Accuracy Analysis of Network-RTK(VRS) for Real Time Kinematic Positioning, Journal of the Korean Society of Surveying, Geodesy, Photogrammetry and Cartography 30(4), pp. 389-396.
- 3) NGII., 2013, A Study for FKP-GPS Service, No. 11-1613436-000016-01, National Geographic Information Institute, Suwon, p. 11.
- 4) Kim, M. and Bae, T., 2015, Preliminary Analysis of Network-RTK for Navigation, Journal of the Korean Society of Surveying, Geodesy, Photogrammetry and Cartography 33(5), pp. 343-351.

Learning Ability of Peace Education Utilized by VR Materials

Soichiro Higuchi* and Byungdug JUN**

ABSTRACT: At 11:02 a.m. on August 9, 1945, the atomic bomb "Fat Man" exploded over Nagasaki City, killing about 73,884 citizens. Tested various educational attempts were on this horrific event to future generations. In particular, "storytelling" by Hibakusha (atomic bomb survivors) was an effort to convey what they experienced at the time vividly. There will inevitably be fewer and fewer opportunities to hear the "real voices" of the Hibakusha soon. We will inevitably lose the chance to listen to the "voices" of Hibakusha shortly. It is a need for a new tool to apply for peace education of atomic bombings. This study aims to create a new peace education tool named "Nagasaki Flight." This tool can use as an alternative to "storytelling." Experience of the image of the change in the city of Nagasaki before and after the atomic bombing using VR goggles gives learning effects. In addition, we hope to develop this content to have non-Japanese people, especially Americans. We hope to compare the difference in user experience between Japanese and non-Japanese people through this result.

Keywords: keyword¹; peace education, atomic bomb, nagasaki

1. Introduction

There are several previous research about this study. Firstly, there was a study of "The GIS project of Peace and Multicultural Education in Nagasaki" by Jun. In this study, the aerial photographs taken by the U.S. military before and after the atomic bombing were pictured and applied on reconstructed maps of the disaster area prepared by the city of Nagasaki based on the city maps. And a three-dimensional bird's-eye view of the streets within a radius of 1 km from the hypocenter in Matsuyama-machi, Nagasaki City, was displayed.

Secondly, there was a study of "3D Reconstruction of Nagasaki used by LPS software around Urakami village of atomic bomb before and after" by Sakaguchi. In this research, extracted 3D data was from aerial photographs of Nagasaki taken by the U.S. military on August 7 and 10, 1945, aiming to use the data as teaching material for peace. The developed 3D data viewer used the Leica Photogrammetry Suite (LPS).

Thirdly, there was a study by Setozaki of "Development of the Spherical Panorama VR Learning Equipment for Peace Education." The purpose of this study is to give learners in remote areas a sense of being in Nagasaki, which is the site of the atomic bombing, to encourage them to learn proactively. Using AR/VR technology, a developed teaching material

* Master Degree Student, IAMAS, higusow21@iamas.ac.jp

** Corresponding author, Professor, Nagasaki University, bdjun@nagasaki-u.ac.jp

was that allows learners to experience on a tablet a panoramic image of the entire sky of the hypocenter and other spots now and one month after the bombing.

2. Developed System Overview

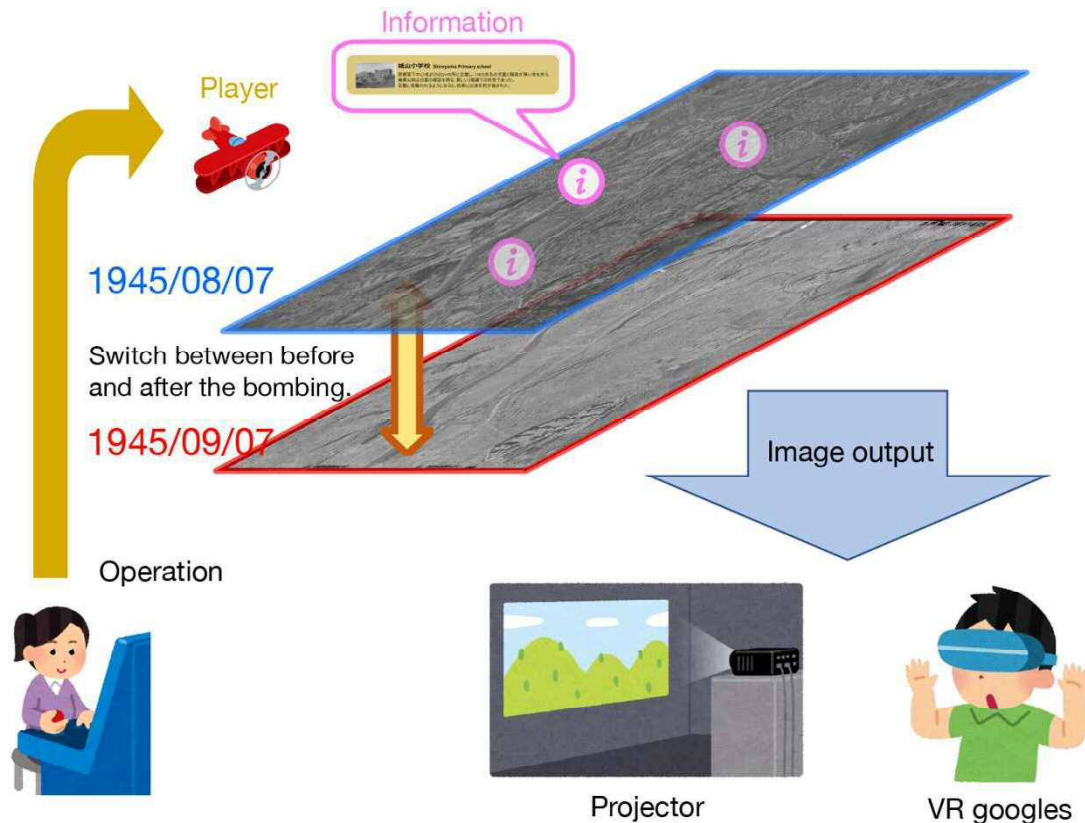


Fig. 1 System overview diagram

Learners operate in pairs to this system. One learner is the pilot and controls the plane with a controller. The pilot uses the aircraft by watching the projected images from the camera behind the aircraft. The other person wears VR goggles. The image projected on the VR goggles is from a camera installed in the airplane's cockpit, and the pilot can simulate the experience of sitting in the cockpit. The flight takes place over Nagasaki City on August 7, 1945 (before the atomic bombing) and September 7, 1945 (after the atomic bombing). Before and after the nuclear bombings can be switched with a button on the controller. Information placed markers are essential for peace education, and when the airplane approaches the locations, the displayed information is on the projector and VR goggles.

The goals of the peace education materials are as follows.

1. To give the user the feeling of being a pilot with a stick-type controller.
2. The VR goggles should give the user an experience as if they are boarding an airplane.
3. The images from the airplane should be enough to compare the urban area before and after the atomic bombing.
4. The location and directions of important spots for peace education should be easy to understand.
5. Additional information spots add quickly.
6. The aircraft should be easy to operate.

7. Two types of airplanes, a small Cessna and a B-29 that dropped the atomic bomb, should be available, and a bird's eye view of Nagasaki city from a U.S. military aircraft of the time provided.
8. It should be available in multiple languages.

2.1 Used Hardware and Software

Table 1 Lists of hardware and software

Hardware	Software
<ul style="list-style-type: none">● Dell Precision7720● Logitech Flight yoke system● HTC VIVE Pro	<ul style="list-style-type: none">● Unity 2019● Microsoft Visual Studio 2019● Agisoft Metashape● Steam VR● Inkscape



Fig. 2 Logitech Flight yoke system (left) and HTC VIVE Pro (right)

2.2 Applied Content-1 (Aerial photographs)

The image of Nagasaki city was from aerial photographs taken by the U.S. military in 1945. This image provided the most accurate and objective depiction of the situation before and after the atomic bombing by using aerial photographs as the source. Scanned aerial photographs were from the film data stored in the U.S. National Archives and Records Administration. Figure 3 shows a photograph of the hypocenter (Matsuyama-machi) area as an example. The right and left photos showed August 7 and September 7, 1945.

2.3 Applied Content-2 (Airplane)

There are two types of planes to be implemented this time: the Cessna and the B-29.



Fig. 3 Aerial photo before and after the atomic bombing (near the Ground zero)



Fig. 4 Composite aerial photo (after the atomic bombing)



Fig. 5 Cessna (left) and B-29 (right)

Using Metashape, multiple photos are superimposed, and the altitude is calculated from the displacement of the camera's viewpoint and converted into a 3D model. In addition, the photographs are pasted onto the 3D model as textures to create 3D data. The obtained topographic data covers an area of about 7 km from north to south (south end: Nani-no-hira-machi and Tategami, north end: Showa-machi and Nijigaoka), and about 4 km from East to the west (east end: Konpira-san and west end: Inasa-Yama), centered around Urakami Station. Figure 7 shows the range. The left side is south (toward Nagasaki Port), and the right side is north (toward Nagasaki University).

2.4 Finalized Execution Content (Nagasaki Flight)

Unity uses a structure called "Scene" to manage the scenes of a game. In this study, we have implemented three locations like bellow lists. (see Fig 6)

1. Title Scene with the logo "Nagasaki Flight"
2. Select Plane Scene (select the plane model to use).
3. Start

Table 2 Lists of information spots and their directions

Spots	Information
Nagasaki Medical College	Because of their wooden construction, 65 of the 76 buildings collapsed and burned down when the bomb exploded. A total of 898 people, including 535 students (about 60% of the total number of students), staff members, doctors, and nurses, died.
Mitsubishi Weapons Ohashi Factory	1.3km north of the hypocenter. It was for the manufacture of torpedoes for the Navy. Together with the Mori-machi factory, the plant employed 17,792 workers, were killed 2,273 workers, and 5,679 were seriously injured.
Shiroyama Elementary School	Located 500 meters from the center of the atomic bombing, more than 1,400 children and staff members lost their precious lives. Before the atomic bombing, the school was a beautiful three-story building with a majestic chalk-white appearance.
Urakami Cathedral	The 26-meter twin towers, built of red bricks for 30 years, were the largest in the East. It collapsed instantly due to the blast, and the roof and floor were lost in the fire.
Yamazato Elementary School	Located 600 meters from the hypocenter, only four of the 32 students enrolled survived. Although no children attended the school that day, the school was severely damaged because the school district was located in the hypocenter zone, and about 1,300 of the 1,581 children in the school died.
Ground zero	171 Matsuyama-cho, Nagasaki City. It is estimated that the bomb exploded at an altitude of 503 ± 10 meters. More than 1,860 people lived in 300 households in Matsuyama-machi. All of them died except for a 9-year-old girl who happened to be in an air-raid shelter.

2.5 Warning Windows

When the plane approaches the ground or a building, a warning message and a warning sound planed to avoid a collision—this warning message displaying on both the projector and the VR goggles. In addition, the plane automatically moves to a place high enough above the collision site.

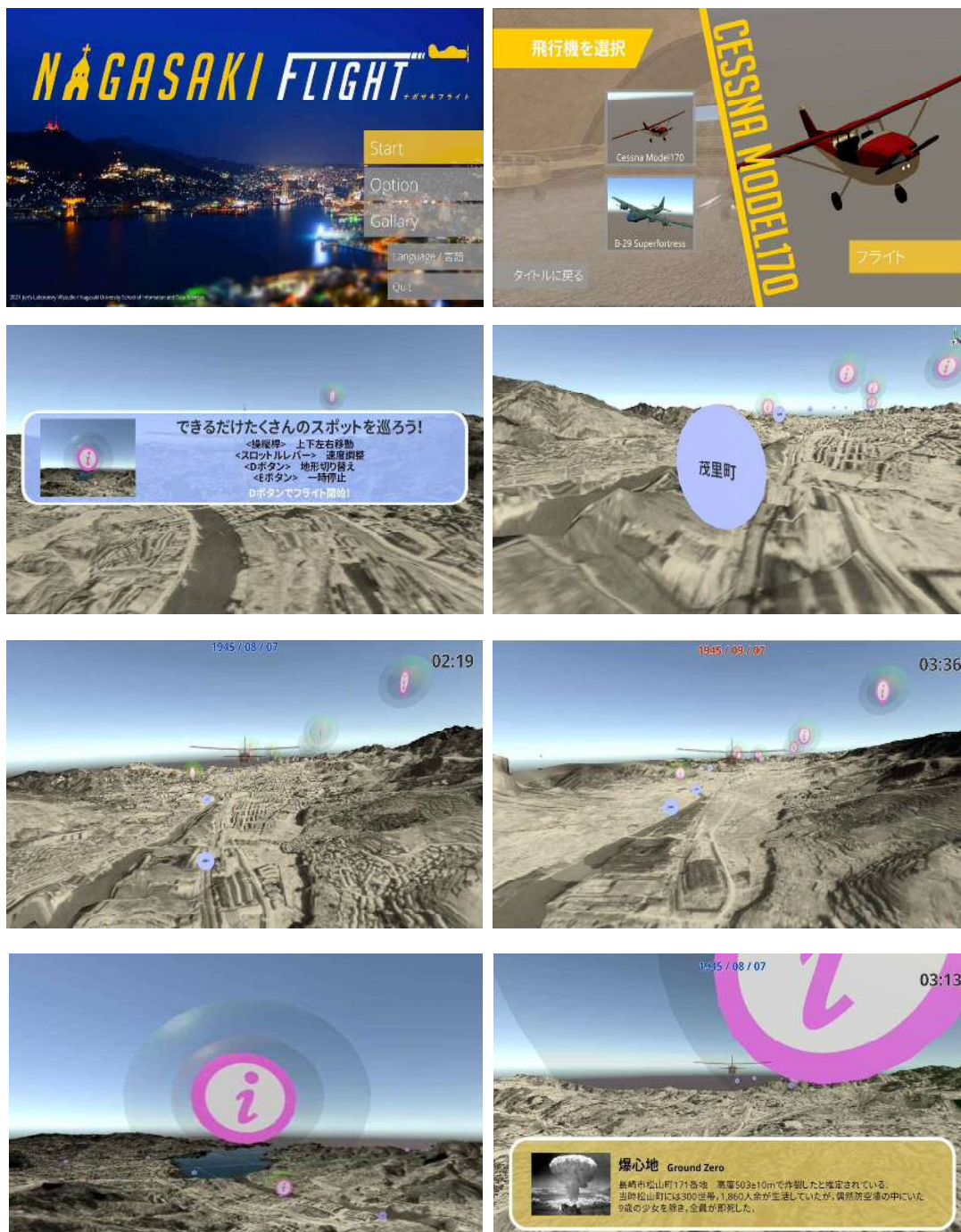


Fig. 6 Cessna (left) and B-29 (right)

3. Experimental Class

To investigate and examine the educational effects of using the produced contents in school, we requested the cooperation of a junior high school attached to the Faculty of Education, Nagasaki University, and conducted a demonstration experiment.

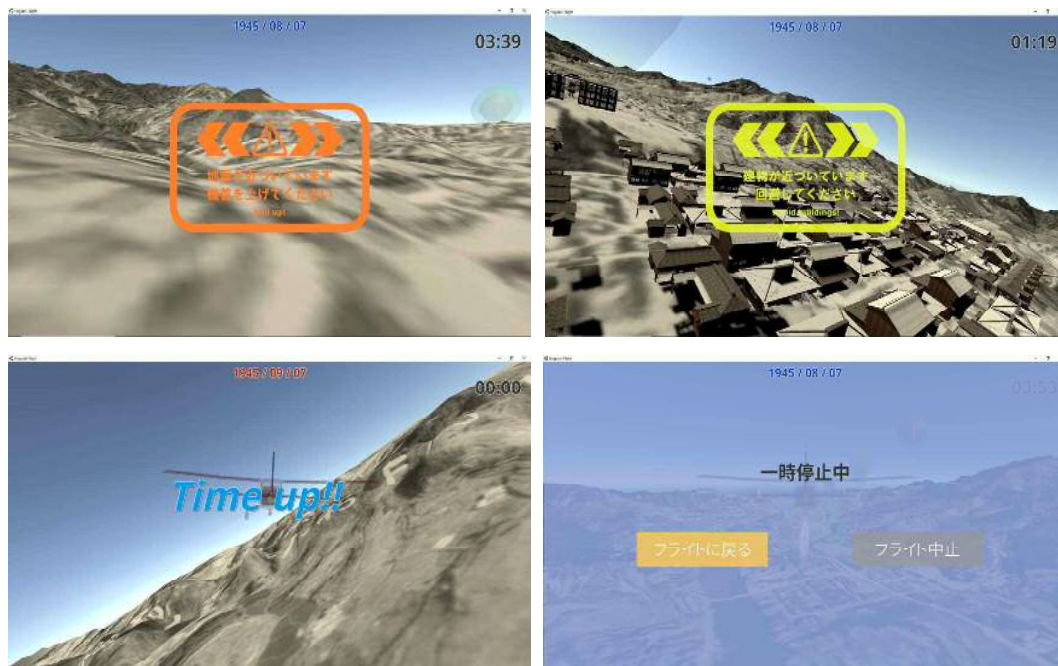


Fig. 7 Examples of warning windows

3.1 Class in School

A fourth-year student of the Faculty of Education taught a class entitled "Using ICT Devices to Understand the History of Nagasaki" as part of a junior high school social studies class and used our system as teaching material. The students tried to learn in pairs, one as the pilot and the other as the VR goggle wearer, and to experience four teams per each class. Four classes were conducted: Class 2, Class 4, Class 1, and lastly, Class 3. The evaluation method was in the form of a questionnaire.



Fig. 8 Experimental class at a junior high school (Nagasaki)

3.2 Questionnaire Survey

The PC screen is projected on display at the front of the classroom. The PC, flight yoke system, and VR goggles were set up in the first row so that the system, the pilot, and the VR goggle wearer could see from anywhere in the classroom. Lastly, we prepared the following questionnaire.

[1]Are you interested in peace education?

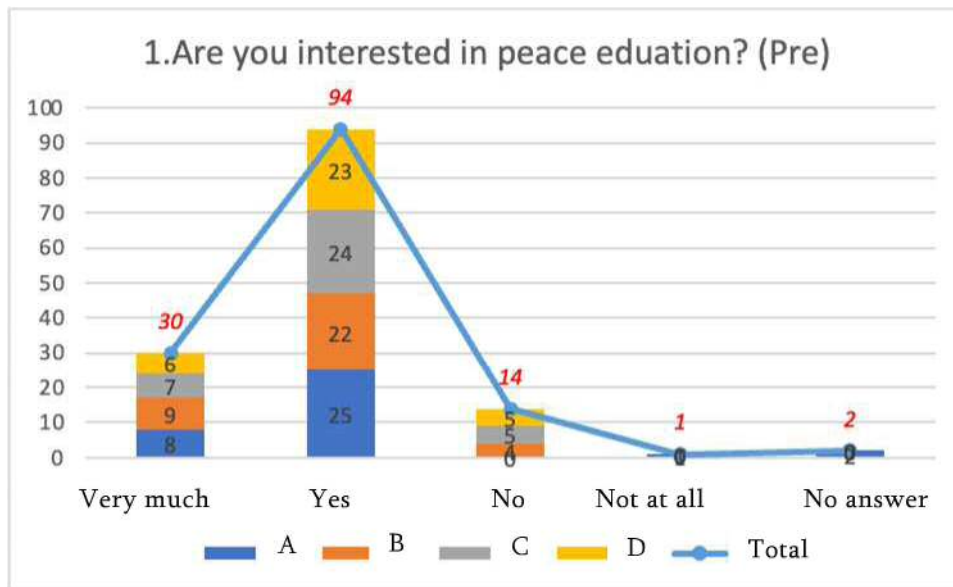


Fig. 9 Pre-questionnaire results 1

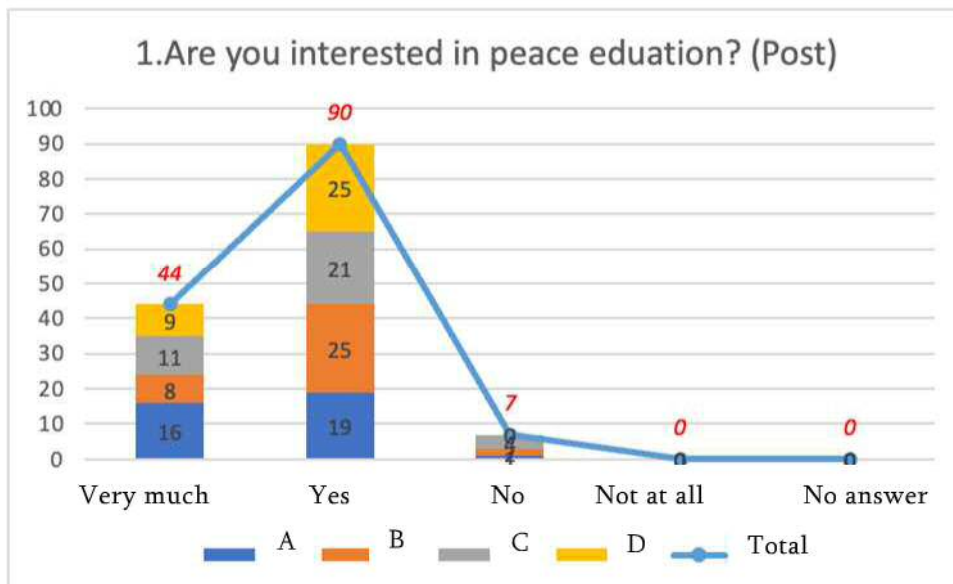


Fig. 10 Post-questionnaire results 1

[2] What do you think about the effects of using ICT equipment in your classes?

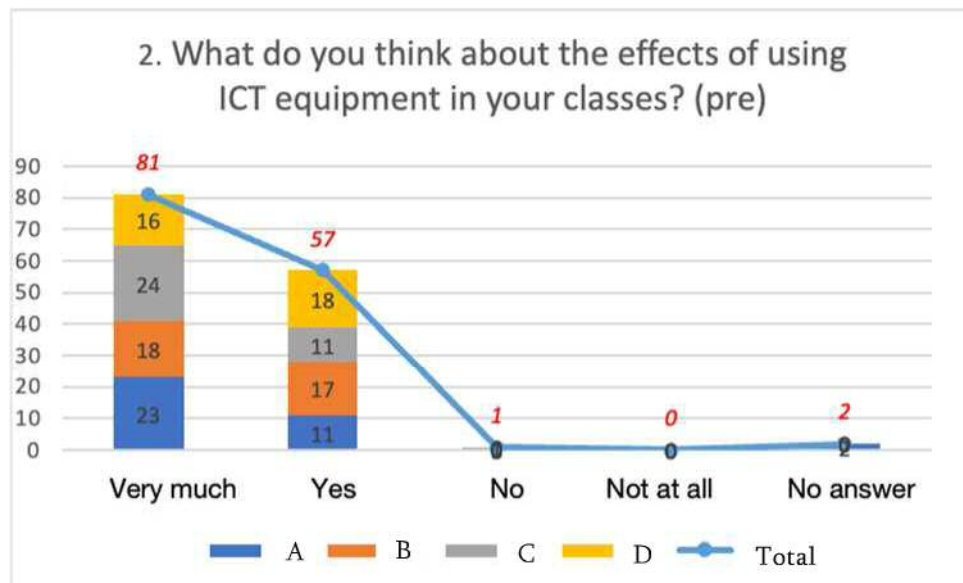


Fig. 11 Pre-questionnaire results

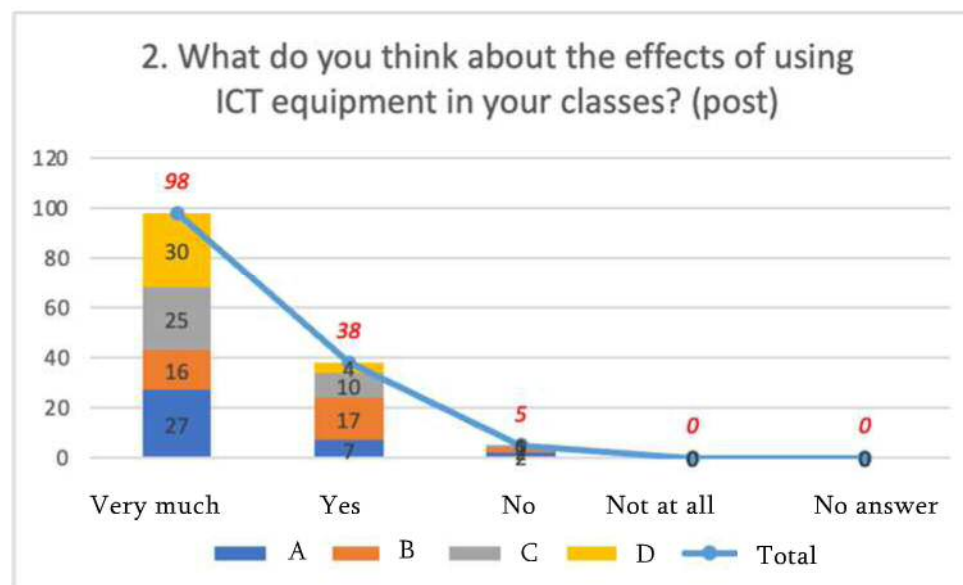


Fig. 12 Post-questionnaire results

4. Conclusion

In this study, we developed "Nagasaki Flight" as a new peace education tool to replace "Storyteller" and evaluate the educational effects of using VR in ICT education. In developing the system, we set the system requirements keeping in mind that the system would be used by people of all ages, both men and women, and of all nationalities. However, this experiment is intended for junior high school students. The system was designed with user experience to encourage active learning while showing the devastation of the atomic bombing through aerial photographs. In

addition, we created the core system to have redundancy so that different information systems can produce for other regions such as Hiroshima, Tokyo, and Pearl Harbor.

The combined control stick controller and VR goggles were generally helpful in terms of the sense of control and realism. On the other hand, some people feel that it is difficult to control the airplane due to its unique characteristics, so it would be better to use the joystick to move the VR camera around in the virtual space rather than piloting an airplane.

As for the learning effects of this teaching material, we can say that the content attracted the learners' interest and provided a different style of teaching material from the conventional peace education. Yet, there are still some problems in using the material in the classroom. And there are still many hurdles for instructors who are not accustomed to handling the equipment in their classes. Therefore, it is necessary to create an easy system for instructors to manage and make instructional plans that effectively use ICT education.

Future tasks are implementing a gallery function to view spot information after the flight. Finally, we hope to evaluate the difference in how the teaching material in Japan and the U.S.

References

- 1) Photos for Atomic bomb of Nagasaki, 1996
- 2) Saying and Pray in Nagasaki 75 years, 2020/08/09 Asahi Newspaper, Chokan
- 3) https://www.mext.go.jp/content/20201218-mxt_kyoikujinzai02-100001263_06.pdf (Date viewed : 2/5/2021)
- 4) (https://www.nier.go.jp/kokusai/pisa/pdf/2018/06_supple.pdf (Date viewed : 2/5/2021)
- 5) (https://www.mext.go.jp/content/20200625-mxt_syoto01-000003278_1.pdf (Date viewed : 2/5/2021)
- 6) Byungdug Jun, Peace and Multi-Cultural Education of Nagasaki, GIS NEXT, Vol.12, pp32-34, 2005
- 7) Jun Sakaguchi and Byungdug Jun, 3D Reconstruction of Nagasaki Used by LPS Software –Around Urakami Village of Atomic Bomb, GISUP 2008 International, pp81-90, 2008.
- 8) Norio Setozaki et. al, Development of peace education materials with spherical panoramic VR content, Jpn. J. Educ. Technol., 39(Suppl.), pp85-88, 2015
- 9) <https://gaming.logicool.co.jp/ja-jp/products/flight/flight-simulator-yoke-system.945-000046.html> (Date viewed : 2/5/2021)
- 10) <https://www.vive.com/jp/product/vive-pro-full-kit/> (Date viewed : 2/5/2021)

Representation of Land Subsidence Analysis Using Interferometric SAR and GIS Technology

Tomohisa Matsuzaki* and Byungdug Jun**

ABSTRACT: The ground deformation around the Tokyo area was observed by interferometric SAR (Synthetic Aperture Radar) in this research. The interferometric SAR is a type of remote sensing watching various information on the earth from satellites. This study compared the SAR data's accuracy with the data obtained by level surveying to examine the accuracy. In addition, we used the GIS function of Google map applying display the changes in ground deformation in an easy-to-understand manner. The results are discussed in this paper.

keyword¹; Interferometric SAR, GIS, Ground deformation

1. Introduction

SAR is an abbreviation for Synthetic Aperture Radar. It is a kind of radar that observes an observation target by periodically irradiating it with electromagnetic waves (microwaves or millimeter waves) from a moving object such as a satellite.

This technology is a type of observation using radar. Electromagnetic waves, known as microwaves or millimeter waves, are periodically irradiated from a moving object in the sky, such as a satellite. The reflected waves are processed to observe the observation target. The SAR technology is a kind of radar-based observation marked by processing the reflected waves. The ground deformation used by radio waves requires a massive antenna. As the name implies, SAR creates a large virtual antenna (aperture) by synthesizing the reflected millimeter-wave waves sent periodically. This technology enables us to obtain observation data with a device mounted on a satellite (see Figure 1).

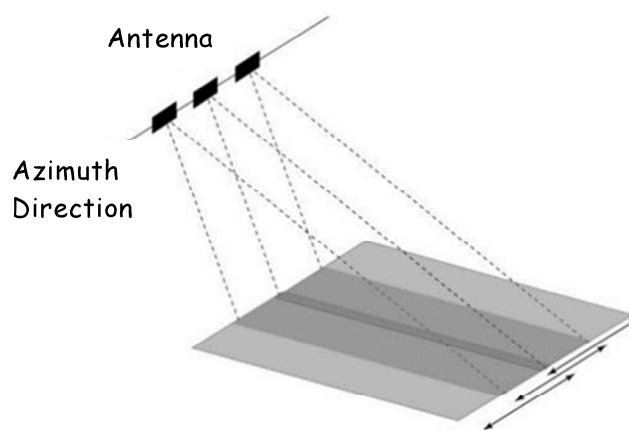


Fig. 1 Observation Diagram used by SAR

* Master Degree Student, Nagasaki University, bb52121317@ms.nagasaki-u.ac.jp

** Corresponding author, Professor, Nagasaki University, bdjun@nagasaki-u.ac.jp

Interferometric SAR is the process of interfering with SAR images obtained on the same plane and under the same conditions (see below). Interferometric SAR is an algorithm to make the variation of the earth surface in two-time series visible by interfering with SAR images obtained on the same plane and under the same conditions (to be described later) and adding some processing. This algorithm makes the variation of the earth surface in two-time series visible by interfering with the SAR images obtained on the same surface information under the same conditions. The principle is the same as that of light interference studied in high school physics. For example, if the same ground area observes two times, a shift in the ground will cause a path difference between the observation point and the satellite. This difference creates a phase difference, and a differential interferometric image can be output.

(1) Observing the same point in the same orbit and direction of travel.

Satellites have a variety of orbits classified as orbital data.

In SAR, the satellite observes the observation point as if it is looking down on it. Therefore, the observation data will look different if the orbit is different, and no interference will occur.

(2) The data must have been observed in the same observation mode.

The SAR sensor has an observation mode with observation resolution, and these modes must match.

(3) The observation periods are not too far apart.

If the observation periods are too far apart, it is impossible to observe detailed ground motion, but the accuracy of the observation data may be insufficient. Therefore, this study set one to two months as the standard observation period.

2 Experimental Survey

We used satellite data obtained from Sentinel-1, SLC (Single Look Complex) as the data acquisition method. The interferometric SAR was applied to measure the Kanto Plain as of 2008 (see Figure 2 for the observation area) in each of the following periods. Use the yellow square to specify the observation range, and select and download the data surrounded by the same red frame to satisfy the conditions.

The screenshot shows a web-based search interface titled 'Advanced Search'. It features several input fields and dropdown menus for filtering satellite data. The 'Sort By' dropdown is set to 'Ingestion Date' and 'Order By' is set to 'Descending'. The 'Sensing period' is defined by two date inputs: '2018/01/01' and '2018/12/31'. Below this, there are empty fields for 'Ingestion period'. The 'Mission' is set to 'Sentinel-1'. Further down, there are dropdowns for 'Satellite Platform', 'Product Type' (set to 'SLC'), 'Polarisation', and 'Sensor Mode'. At the bottom, there is a text input for 'Relative Orbit Number (from 1 to 175)'. A 'Clear' button is located in the top right corner of the search area.

Fig. 2(a) Windows for Search Inputs

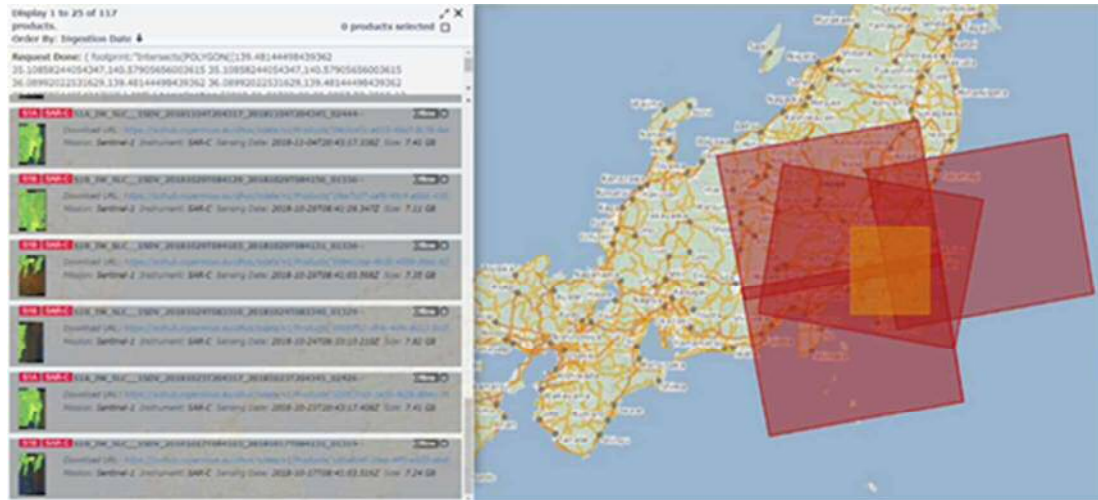


Fig.2(b) Use the website (Copernicus ESA) to input the conditions and obtain data.

(URL:<https://scihub.copernicus.eu/dhus/#/home>)

The following processes were steps of interferometric SAR processing.

(1) Output of intensity and phase images

The obtained data is SLC (Single Look Complex), expressed as a complex number. It is output as the intensity and phase components are extracted and imaged based on format 3.

(2) Image alignment

Based on the output intensity image, the misalignment of the paired image data in the pixel and line directions is estimated.

The output intensity image is used to estimate the paired image data's misalignment in the pixel and line directions. The idea is shifted by the shift determined for the phase image.

(3) interference processing

Interference processing is performed by subtracting the phase images of the aligned pairs. In this process, the photos with darker stripes are regarded as "highly interferometric results," and the final output is more precise.

(4) Removal of orbital fringes

The initial interference image contains several elements, which the following equation can express.

$$\Phi_{data} = \Phi_{orb} + \Phi_{geo} + \Phi_{ifgm} + \Phi_{noise}$$

Φ_{orb} , Φ_{geo} , Φ_{ifgm} , and Φ_{noise} represent orbital fringes, topographic fringes, interference fringes, and noise, respectively. The other three need to remove because the final goal is to keep only the interference fringes. In this stage, we will remove the orbital boundaries Φ_{orb} , which are the fringes caused by the satellite's movement. The idea assumes that the earth is an ellipse with no irregularities. In this case, the stripes caused by the path difference (ΔR) between the earth's surface and the satellite are regarded as orbital fringes. (See Figure 3)

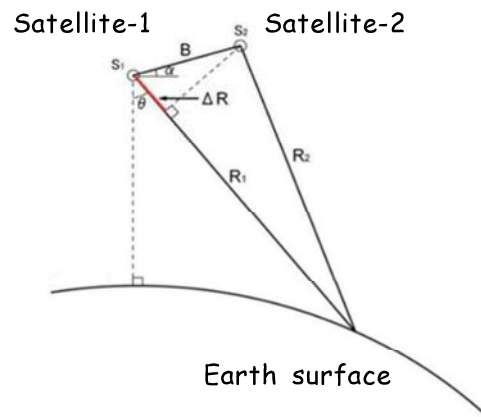


Fig.3 the path difference ΔR that causes orbital stripes

ΔR is the path difference between the two scenes, from which the phase difference calculated the orbit fringes. The expression of the phase difference is expressed as $4\pi \cdot \Delta R / \lambda$. After the orbit fringes are generated, they are removed by subtracting the initial interference image.

(5) Removal of topographic stripes

As the name implies, topographic stripes are stripes derived from the topography of the observation point. Since topographic stripes can be regarded as coincident at the same issue, they can be removed by subtracting two "initial interferogram with orbital stripes removed."

The topographic stripes can be removed by subtracting the two "initial interferogram with orbital stripes removed." The topographic fringes can be removed by subtracting the two "initial interferogram with orbital fringes removed." By performing the above process, a differential interferogram can be generated.

(6) Noise removal

Since reflected waves are used for measurement, data (noise) that is not the waveform to be observed may be included. To prevent this, the data is usually filtered to remove the noise.

(7) unwrapping

The differential interferometric image obtained through the process described in step 7 is unwrapped in the range of 0 to 2π in phase, so the correct amount of variation is obtained by guessing from the reference point.

The named "SNAP" software was used to perform the above (1)~(6) process.

The Algorithm named "SNAPHU" was used to unwrap phase data.

The data after the unwrapping process looks like the following. We will make the colors outside the terrain transparent for the image and output it as a kml file. The SAR processed file as a kml file will be carried out for the following pairs of periods. (Jan. 8 - Feb. 25, Feb. 25 - Mar. 21, Mar. 21 - May 20, May 20 - Jul. 19, Jul. 19 - Sep. 5, Sep. 5 - Oct. 23, Oct. 23 - Nov. 16, Nov. 16 - Dec. 22)

The year 2008 in the Ministry of the Environment's overview of land subsidence in Japan [reference 2)] is suitable as a reference as data to confirm the accuracy of the analysis results. We will calculate the subsidence amount by accumulating the subsidence obtained by interferometric SAR. These results compare how far it is from the reference data. In this research, we will take for the area around Tokyo.

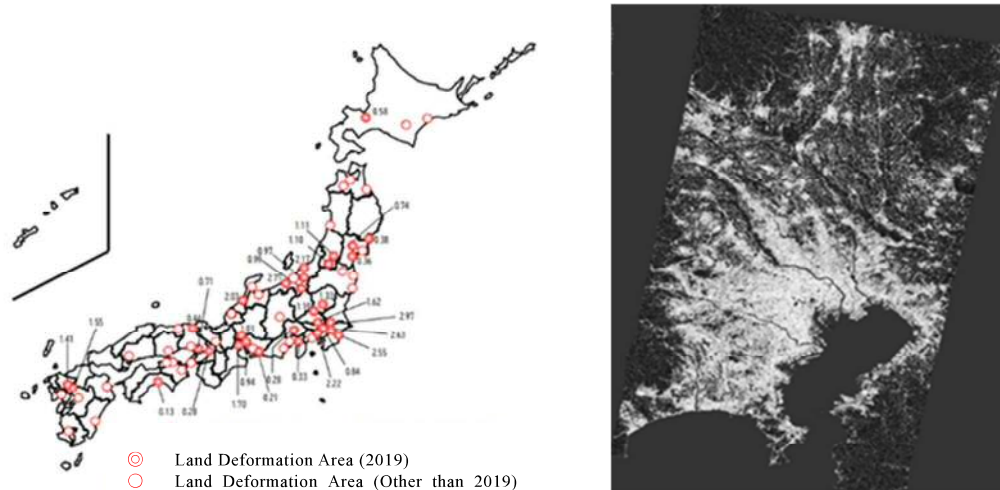


Fig.4 Approximate land subsidence status and actual observation range

The four observation points are Yokohama (latitude: 35.4471, longitude: 139.6399), Tokyo (latitude: 35.6810, longitude: 139.7690), Saitama (latitude: 35.8611, longitude: 139.6414), and Chiba (latitude: 35.6068, longitude: 140.1058). (latitude: 35.6068, longitude: 140.1058), and Chiba (latitude: 35.6068, longitude: 140.1058), respectively. These data were from by level surveying not obtained by interferometric SAR. In this paper, we try to compare the level survey and SAR results. We are checking the accuracy of the interferometric SAR. Precisely, we will determine the land subsidence for one year by connecting the data obtained by interferometric SAR generated at intervals of one to two months. In other to obtain the data of the corresponding observation area accurately, the phase data (data of ground deformation) assigned to one pixel of the unwrapped data is obtained by comparing it with the location information of the unwrapped data and compared with the data obtained by level surveying. Refer to the seasonal trends in ground deformation "2008 Ground Subsidence and Groundwater Level Observation Information". [reference 2)]

As for the seasonal trend of ground deformation, it realized that the result could be produced "the tendency of sinking during summer and offsetting the sinking during summer by uplift in autumn" is the same in each region, as shown on page 12 of it.

3. Results

Finally, the ground deformation in the test area was calculated by interferometric SAR processing. The results are as follows. Yokohama (- 1.9cm), Tokyo (- 0.635cm), Saitama (- 1.54cm), Chiba (- 1.8cm) (Results of level survey values are -2.22cm, -0.84cm, -1.62cm, -2.63cm) In comparison with the level survey values, Yokohama has a bias error of 0.32 cm, Tokyo 0.205 cm, Saitama 0.08 cm, and Chiba 0.8 cm, relatively. The Chiba has a large number of bias errors. It is necessary to examine this issue by comparing the data obtained from the interferometric SAR analysis with the data obtained from the areas surveyed quickly.

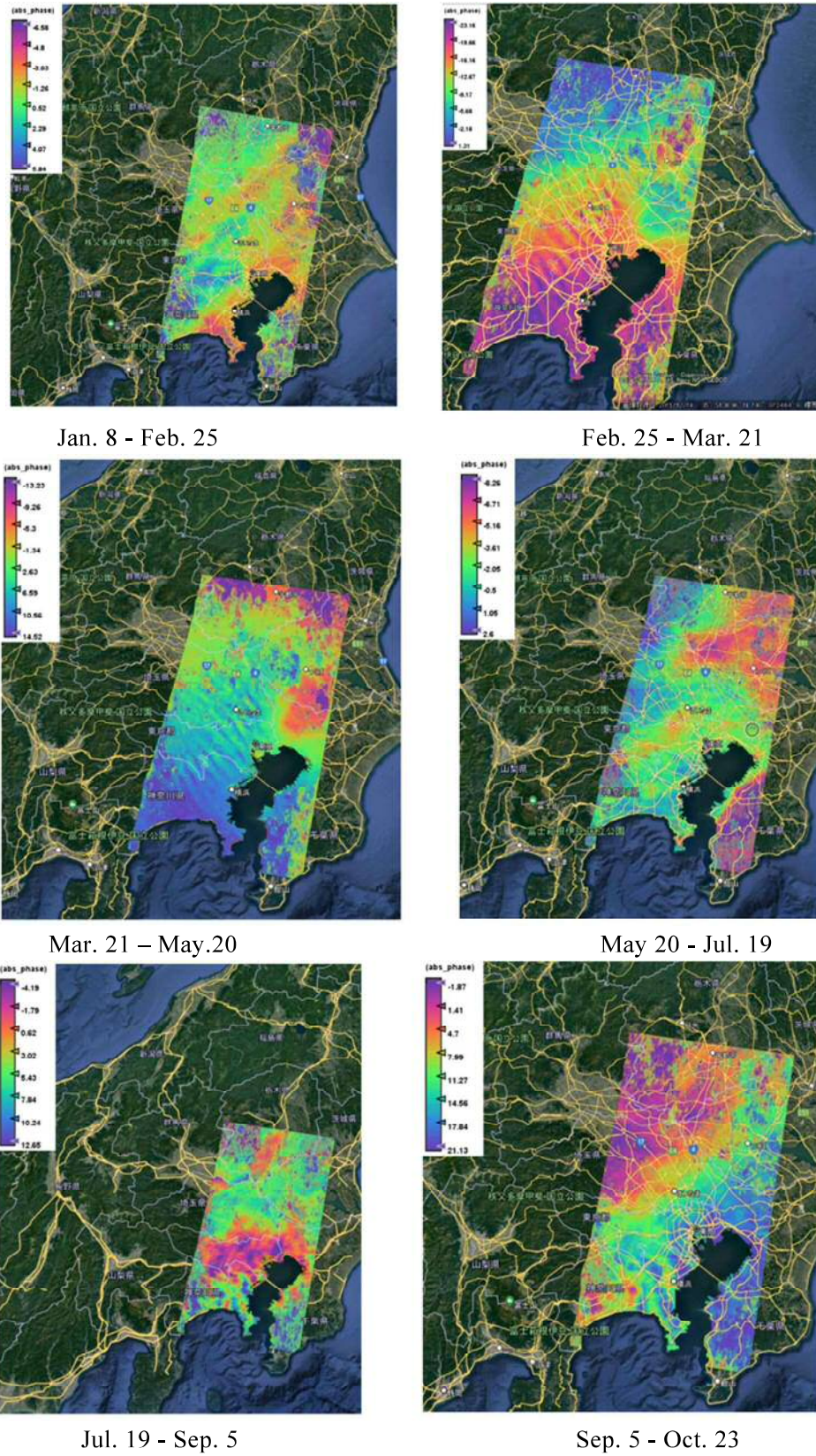
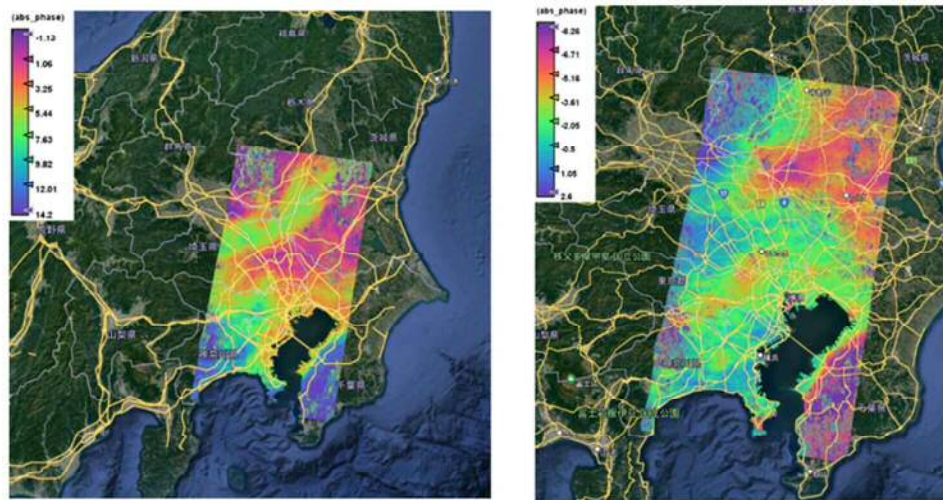


Fig.5(a) Approximate land subsidence status and actual observation range



Oct. 23 - Nov. 16

Nov. 16 - Dec. 22

Fig.5(b) Approximate land subsidence status and actual observation range



Fig.6 Layer structure

On the other hand, we have to think about the "tendency for land subsidence to subside during the summer season and for the uplift in the autumn season to offset the subsidence in the summer season." For this comment, we are used data from Yokohama as an example. The amount of ground deformation from the observation period in January analyzed by interferometric SAR is as follows. All units are in mm. (-23.32482, -2.521337, 9.88284, -21.20549, 5.00021, 9.80965, 5.47891, -2.949993)

Except for March to May and November to December, the approximate trend is the same as the above comment. Therefore, from these results, we could conclude that the applied GIS technique is able to show a general trend, although it lacks detailed accuracy.

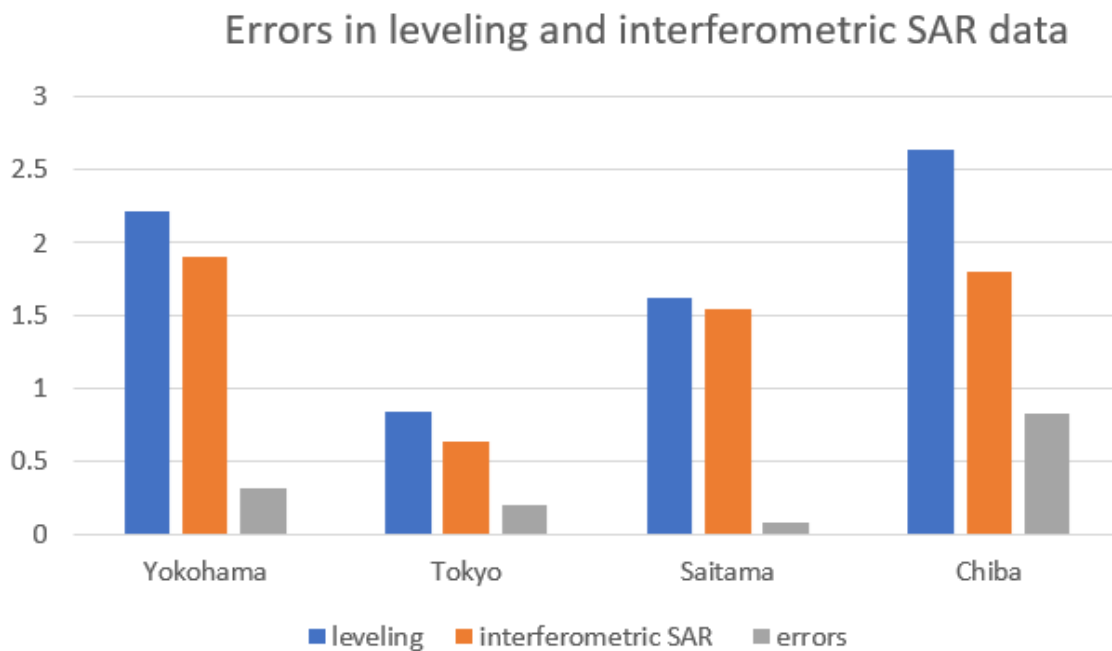


Fig.7 Vias Errors in leveling and interferometric SAR data

4.Discussion

In the future, we would like to verify with more in-situ data. Furthermore, we hope to increase the GIS layer and express the effect of visual SAR data.

References

- 1) User Guides - Sentinel-1 SAR - Mapping of Applications to Sentinel-1 Modes – Sentinel Online, <https://earth.esa.int/web/sentinel/user-guides/sentinel-1-sar/applications/mapping-applications-s1-modes>
- 2) 2008 Ground Subsidence and Groundwater Level Observation Information, <https://www.pref.saitama.lg.jp/documents/25418/h30nenpou.pdf>
- 3) The year 2008 in the Ministry of the Environment's overview of land subsidence in Japan <https://www.env.go.jp/water/jiban/chinka.html>
- 4) Satellite Applications Manual for Land Subsidence Observation - Ministry of the Environment, <http://www.env.go.jp/press/files/jp/105895.pdf>

Colorization of the Historical Aerial Photography with AI “DeOldify”

Yuta Umeda* and Byungdug Jun**

ABSTRACT: Many colorized pictures have been produced and shown in various sites with AI engines. It is turning black and white photos into color in seconds. Especially reimagining the past by colorizing photographs and historical figures has a significant impact. Almost all pictures colorized are targeted to portrait or landscape photos. The historical aerial photography is mere. In this paper, we want to introduce the model for colorization of the historical aerial photograph with AI. Plans also are discussed.

Keywords: keyword¹; colorization, historical areal photograph, nagasaki

1. Introduction

"Development and practice of VR content for peace learning using photogrammetry technology " is the title of our lab's pre-research using VR goggles. It was conducted in all laboratories last year. We decided to take over last year's pre-research and improve it with more versions for learning content. In addition, we challenged colorizing the 3D models to improve them as peace learning content. Therefore, I focused on the artificial intelligence "DeOldify" in the public library this time. DeOldify is an image processing with AI that uses deep learning. It is an AI of a colorization program that anyone can use on Google Colaboratory. Moreover, it supports complicated colors such as national costumes from all over the world with high accuracy. In this research, we will perform colorization using DeOldify.

2. Experiment

Firstly, we decided to colorize the aerial photograph taken on May 5, 1973, centering on Matsuyamamachi, Nagasaki City, using DeOldify. As we mentioned before, the reason for colorizing the aerial photo of 1973 is best to close the oldest color aerial photograph of Nagasaki City owned by the Geographical Survey Institute, which was taken on March 8, 1975. Therefore, we tried to check the accuracy by colorizing the aerial photograph of 1973. We tried to join the previous research by referring to the paper "Colorization of aerial photographs taken by the US military and its evaluation." The content of this paper is briefly explained by dividing a black-and-white image into vegetation categories and colorizing each vegetation category using the gradation values of the black-and-white image. In this paper, they used the application of "Illustrator," but we used the application of "Pro Create" because we wanted to work on the iPad.

The following steps are a method of colorizing black-and-white aerial photographs. Firstly, because of the enormous size image (see Figure 1), the aerial photograph cannot be colorized by DeOldify, so the image is cropped to a size that can be read by DeOldify (The size of the image is about 720 x 483).

* Undergraduate Student, Nagasaki University, bb35318009@ms.nagasaki-u.ac.jp

** Corresponding author, Professor, Nagasaki University, bdjun@nagasaki-u.ac.jp

Here, a slight groove is created between the images to be cropped when cropping an aerial photograph, as shown in Figure 2. The previous paper is used when stitching the cropped images together. If the image is cropped, as shown in Figure 2, it becomes challenging to join the colors colored by DeOldify at the joint between image A and image B when they become different colors. It is by intentionally making a slight groove, as shown in Figure 2. Figure 3 is final image.

Here, the cropped image is colored by DeOldify. Then, how this ditch was colored is classified into eight types: forests, logging areas, rivers, bare land, railroads, roads, private houses, and unique buildings. As a color sample corresponding to each, it is taken from either the upper or lower image trimmed and colored by DeOldify from the dropper function of "Pro Create" and colored using the gradation value of the black-and-white image. After that, each image is joined, and the groove is colored by the above method to complete the image.



Fig. 1 Original size photo

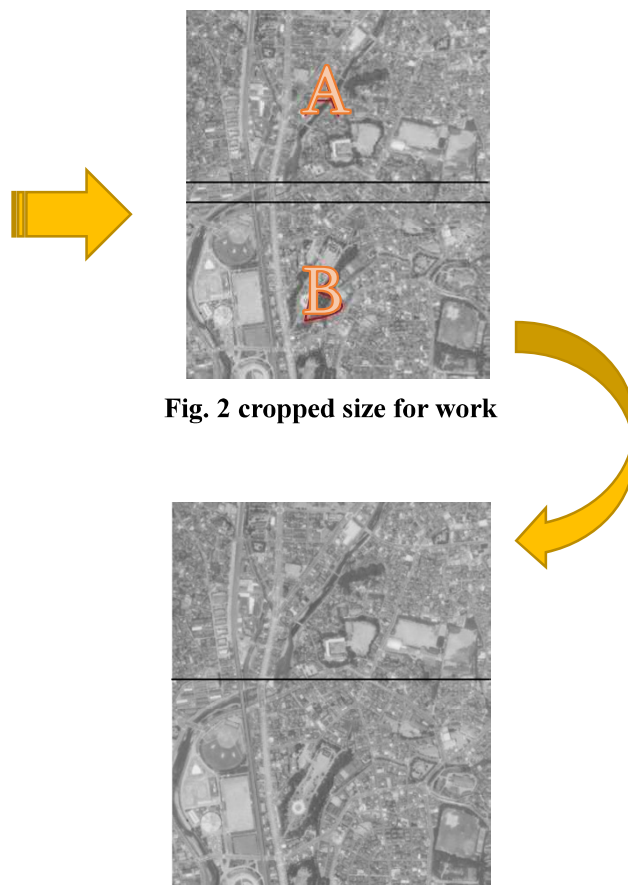


Fig. 2 cropped size for work

Fig. 3 Final result after work

Figure 4 shows the colorized aerial photograph completed in this way. Figure 4 on the left is a color aerial photograph of Nagasaki City in 1975. Comparing Figures 4 (left and right), the overall color scheme is different, but the color scheme and the like seem almost identical.

3. Results and Discussion

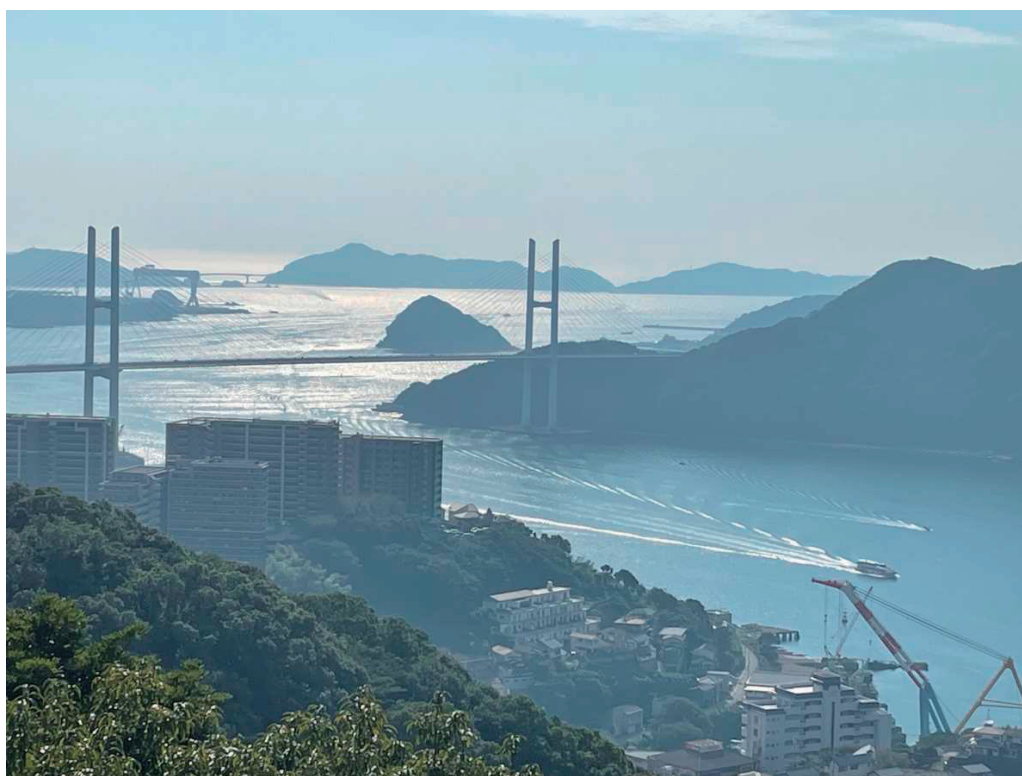
Although it was manual work at this time, we could colorize it. Therefore, we thought various aerial photographs could be colored using this technology. However, there is some problem in colorizing the overlapped area. We hope to use this colorization photograph for peace education in class.



Figure 4 Completed color aerial photograph (left: Original color, right: composite color)

References

- 1)NHK Broadcasting Culture Research Institute "Memory that fades 70 years after the atomic bomb was dropped, how to pass it on"
https://www.nhk.or.jp/bunken/research/yoron/20151101_5.html
- 2)Hiroyuki Hasegawa, Ryoichi Koshirai, Hiroshi Sato, Akiko Iizumi ,Colorization of aerial photographs taken by the US military and their evaluation, JSPRS, Vol.44, No.3, , pp 23-36, 2005



Named "MEGAMI" one of the big bridge, called "Megamioohashi"